# Improved decomposed-coordinated Kriging modeling strategy for dynamic probabilistic analysis of multi-component structures

Cheng Lu[a], Yun-Wen Feng[a], Cheng-Wei Fei [b,c,*], Si-Qi Bu[c], Yat-Sze Choy[d]

[a]School of Aeronautics, Northwestern Polytechnical University, Xi'an, 710072, P.R. China

[b]School of Transportation Science and Engineering, Beihang University, Beijing 100191, P.R. China

[c]Department of Electrical Engineering, The Hong Kong Polytechnic University, Kowloon, Hong Kong, P.R. China

[d]Department of Mechanical Engineering, The Hong Kong Polytechnic University, Kowloon, Hong Kong, P.R. China

**Abstract**: The probabilistic design of complex structure usually involves the features of numerous components, multiple disciplines, nonlinearity and transients, and thus requires a lots of simulations as well. To enhance the modelling efficiency and simulation performance for the dynamic probabilistic analysis of multi-component structure, we propose an improved decomposed-coordinated surrogate model method (IDCSMM), by integrating decomposed-coordinated (DC) strategy, extremum response surface method (ERSM), genetic algorithm (GA) and Kriging surrogate model. The GA is to resolve the maximum likelihood equation (MLE) and achieve the optimal values of the Kriging hyperparameter $\boldsymbol{\theta}$. The ERSM is utilized to resolve the response process of outputs in surrogate modeling by extract the extremum values. The DC strategy is used to coordinate the output responses of analytical objectives. The probabilistic analysis of an aeroengine high-pressure turbine blisk with blade and disk is conducted to validate the effectiveness and feasibility of this developed method, by considering fluid-thermal-structural interaction. In respect of this investigation, we see that the reliability of turbine blisk is 0.9949 as the allowable value of radial deformation is $2.310\times10^{-3}$ m. In term of the sensitivity analysis, the highest impact on turbine blisk radial deformation is gas temperature, followed by angular speed, inlet velocity, material density, outlet pressure and inlet pressure. By the comparison of methods (IDCSMM, the DCSMM with quadratic polynomial (QP-DCSMM) and the DCSMM with Kriging (K-DCSMM), and the direct simulation (FE/FV) with the MC method) from the model-fitting features and simulation performance perspectives, we discover that the developed IDCSMM is superior to the other three methods in the precision and efficiency of modeling and simulation. The efforts of this study provide a high-efficient and high-accurate technique for the dynamic probabilistic analysis of complex structure and enrich mechanical reliability theory.

**Keywords**: dynamic probabilistic analysis; improved decomposed-coordinated surrogate model method; multi-component structure; turbine blisk

## 1 Introduction

Complex structure is always assembled by many components with respect to specific rule, and is also called multi-component structure. The assembly relationships among components not only affect the performance of the structure under system working [1]. A component fault emerged in operation is to lead to the failure of the whole system [2]. To keep structure security by designing the assembly relationships, it is urgent to study the dynamic probabilistic analysis of multi-component structures in respect of run status and random parameters.

Lots of investigations have focused on the analysis and design of multi-component structure. Whitney et al.,[3] discussed the design of assemblages based on the new synthesis theory with prior knowledge. Cai et al.,[4] studied the mechanical behavior of cable-strut structures with symmetrical and asymmetrical load cases. Qian et al.,[5] proposed an intelligent approach based on finite element (FE) analysis and artificial neural networks (ANN), to analyze the performance of complex structure. Salehyar et al.,[6] studied a coupled aero-hydro-elastic numerical

---
* Corresponding author. C.-W. Fei
  Email address: feicw544@163.com.

model to investigate the dynamic response for floating wind turbine with non-periodic disturbances. Demoly et al.,[7] developed a novel method for an integrated assembly modeling and planning to design the relevant parameters of products. Liu et al.,[8] analyzed the assembly precision with component deformations based on Jacobian-torsor model by considering temperature, gravity and working loads. Khorrami et al.,[9] adopted the modified harmonic balance method to investigate the vibration response characteristics for rotor disc-bearing. Huang et al.,[10] studied the nonlinear torsional vibration properties of an internal combustion engine crankshaft. Chakravarthy et al.,[11] discussed the frequency characteristics of an aero-elastic wing multi-component structure in the time domain for designing structural parameters. Ma et al.,[12] utilized an improved dynamic model to implement the vibration analysis of a rotor-blade system with blade-tip rubbing based on FE method. The above works keep a watchful eye on the multi-component structural characteristics based on static and dynamic deterministic analysis without the consideration of the effects of random factors. Actually, most of influencing factors have strong randomness on the property of multi-component structure in engineering practice. Hence, the randomness of parameters needs to be considered to study the reliability of multi-component structure from a probabilistic perspective. Only in this way, can the reliability and performance be more precisely evaluated and the related parameters be designed for multi-component structure.

Up to now, a number of literatures have emerged on the probabilistic analysis of multi-component structure by considering the randomness of related variables, and developed various analytical techniques. Birnbaum et al., [13] analyzed the performance of multi-component system and evaluating their reliability by FE method. Gheisi et al., [14] presented a reliability surrogate to discuss the reliability of the water distribution system with multiple components. Gao et al., [15] extended and established the relationship of joint reliability importance and joint failure importance for multi-component system. Schottl et al., [16] developed an analytical model for the reliability evaluation of multi-component structure. Song et al., [17] proposed a novel model to accomplish the multi-component system reliability analysis, by considering an assembled system of degrading components. Heydt et al., [18] applied Monte Carlo simulation to analyze the reliability of distribution system with multiple structures. Fei et al., [1] proposed a methodology, namely distributed collaborative response surface method, for the mechanical dynamical assemble reliability design, and then employed this method in the static and dynamic probabilistic analyses of the radial running clearance of an aeroengine turbine blade in respect of support vector machine [19, 20]. Gao et al., [21] investigated the reliability assessment of turbine blade low-cycle fatigue damage combined with distributed collaborative response surface model. Although the above efforts developed many technologies for the probabilistic analysis of multi-component structure, most works studied the reliability evaluation and sensitivity analysis of multi-component structure without the variation of relevant parameters with time. To deal with the transient problem in dynamic structural probabilistic analysis, extremum response surface method (ERSM) [24, 25] and extremum response surface model-based support vector machine regression [22] have sprung up in recent years. However, the transient issue in the dynamic probabilistic analysis of multi-component structure cannot still effectively to be addressed. In this case, Fei et al., [1, 26] developed the distributed collaborative ERSM based on quadratic polynomials, for the dynamic structural probabilistic analysis with multiple components. This method still suffers from low computational accuracy and efficiency owing to the limitation of quadratic polynomials.

In this work, an efficient and precise analytical technique is proposed to evaluate the dynamic reliability and sensitivity of multi-component structure, based on decomposed-coordinated (DC) strategy, ERSM and improved Kriging (IK) algorithm which introduces genetic algorithm (GA) into Kriging surrogate model. We call this method as improved decomposed-coordinated surrogate model method (IDCSMM). This method is used to finish the dynamic probabilistic analysis of an aeroengine turbine blisk radial deformation, by considering fluid-thermal-structure interaction. The feasibility and applicability of the method are verified by means of the comparison of

different analytical methods.

In what follows, Section 2 elaborates the basic principles of IDCSMM for the dynamic probabilistic analysis. In Section 3 the reliability evaluation and sensitivity analysis of the turbine blisk radial deformation of aeroengine high pressure, which is assembled by blade and disk, are performed using the IDCSMM, under considering the influence of random inputs, such as inlet velocity, inlet pressure, outlet pressure, gas temperature, angular speed, material density, and so on. Section 4 validates the superiorities of the developed method in modeling accuracy and simulation efficiency. Some conclusions of this effort are summarized in Section 5.

## 2 Basic theory

This section gives an overview of the Kriging surrogate model is firstly presented. Then the basic principles of IK algorithm and IDCSMM are discussed. Next, the dynamic probabilistic analysis of multi-component structure is described based on the proposed method. Lastly, the detailed procedure of dynamic reliability evaluation and sensitivity analysis for multi-component structure is elaborated.

### 2.1 Kriging surrogate model

Kriging surrogate model was firstly emerged in the field of geostatistics by Krige [27], and Matheron developed the concept of geostatistics and employed the Kriging surrogate model to deal with the problems of mineral deposit reservation and error estimation subsequently [28]. In recent years, the Kriging surrogate model has been widely used in various areas, such as structural design optimization [29, 30], modeling approximation [31-33], structural probabilistic analysis [34, 35], and so forth. It is demonstrated that the Kriging surrogate model can accurately and effectively handle the problems of high-nonlinearity and high-dimension with large scale parameters.

The form of the Kriging model contains two parts, namely a liner regression of the data and a realization of the stochastic process [28, 36, 37], which is shown as follows

$$Y(\boldsymbol{x}) = \sum_{i=1}^{k} f_i(\boldsymbol{x})\beta_i + Z(\boldsymbol{x}) = \boldsymbol{f}^{\mathrm{T}}(\boldsymbol{x})\boldsymbol{\beta} + Z(\boldsymbol{x}) \tag{1}$$

here $i=1, 2, \cdots, k$; $\boldsymbol{f}(\boldsymbol{x}) = [f_1(\boldsymbol{x}), f_2(\boldsymbol{x}), \cdots, f_k(\boldsymbol{x})]$ is the vector of $k$ basis functions; $\boldsymbol{\beta} = [\beta_1, \beta_2, \cdots, \beta_k]$ is the vector of $k$ undetermined coefficients; $Z(\boldsymbol{x})$ is the stochastic component. Hereinto, $Z(\boldsymbol{x})$ is regarded as the realization of a standard Gaussian random function with expected value $E[Z(\boldsymbol{x})]=0$, and covariance can be denoted as:

$$Cov\left[Z(\boldsymbol{x}_p), Z(\boldsymbol{x}_q)\right] = \sigma^2 R(\boldsymbol{\theta}, \boldsymbol{x}_p, \boldsymbol{x}_q) \tag{2}$$

in which $R(\cdot)$ indicates the correlation function with $R(0)=1$; $\sigma^2$ represents the variance; the Kriging hyperparameter $\boldsymbol{\theta}$ shows the vector of correlation parameters, which is formed by $\boldsymbol{\theta}=\{\theta^{(j)}\}$, $j=1, 2, \cdots, n$, $n$ is the number of inputs; $\boldsymbol{x}_p$ and $\boldsymbol{x}_q$ denote the vectors of the $p$-th and $q$-th samples of input variables, here $p, q=1, 2, \cdots, m$, $m$ is the number of samples.

The correlation function $R(\cdot)$ in Eq.(2) typically satisfies the product correlation rule in the Kriging surrogate model, the form of one-dimensional correlations can be written as a product of stationary [36], i.e.,

$$R(\boldsymbol{\theta}, \boldsymbol{x}_p, \boldsymbol{x}_q) = R(\boldsymbol{\theta}, \boldsymbol{d}) = \prod_{j=1}^{n} R_j\left(\theta^{(j)}, d_{pq}^{(j)}\right) \tag{3}$$

where $R_j\left(\theta^{(j)}, d_{pq}^{(j)}\right)$ is the correlation function of the $j$-th component; $d$ is the vector of distance between two

points; $d_{pq}^{(j)} = \left|x_p^{(j)} - x_q^{(j)}\right|$ is the distance between $p$-th and $q$-th points in $j$-th dimension, in which $x_p^{(j)}$ and $x_q^{(j)}$

are the $j$-th component of the $p$-th and $q$-th input samples; the correlation parameters (Kriging hyperparameters) $\theta^{(j)}$ are called length scale or distance weight, which is typically obtained via the maximum likelihood estimation (MLE) algorithm.

The correlation function is generally formed by a linear, cubic, exponential, spline, Gaussian correlation function and so forth [38], the forms of which play an important role on the accuracy of a Kriging surrogate model. The Gaussian correlation function is selected as the kernel function in this study for its excellent computing performance [38, 39]. The formula of the Gaussian correlation function is

$$R(\boldsymbol{\theta}, \boldsymbol{d}) = \exp\left(-\sum_{j=1}^{n} \theta^{(j)}\left(d_{pq}^{(j)}\right)^2\right) \tag{4}$$

With regard to the MLE algorithm, the parameters $\boldsymbol{\beta}$, $\boldsymbol{\theta}$ and $\sigma^2$ in Eqs.(1)~(4) are derived, i.e.,

$$\max \quad L(\boldsymbol{\theta}) = -\left(m\ln\left(\hat{\sigma}^2\right) + \ln\left[\det(\boldsymbol{R})\right]\right) \tag{5}$$

in which $\hat{\sigma}^2$ is the estimated variance; $\boldsymbol{R}$ is the correlation matrix. The forms of $\hat{\sigma}^2$ and $\boldsymbol{R}$ are

$$\hat{\sigma}^2 = \frac{1}{m}(\boldsymbol{Y} - \boldsymbol{F}\boldsymbol{\beta})^{\mathrm{T}}\boldsymbol{R}^{-1}(\boldsymbol{Y} - \boldsymbol{F}\boldsymbol{\beta})\boldsymbol{\beta} \tag{6}$$

$$\boldsymbol{R} = \begin{bmatrix} R(\boldsymbol{\theta}, \boldsymbol{d}_{11}) & R(\boldsymbol{\theta}, \boldsymbol{d}_{12}) & \cdots & R(\boldsymbol{\theta}, \boldsymbol{d}_{1m}) \\ R(\boldsymbol{\theta}, \boldsymbol{d}_{21}) & R(\boldsymbol{\theta}, \boldsymbol{d}_{22}) & \cdots & R(\boldsymbol{\theta}, \boldsymbol{d}_{2m}) \\ \vdots & \vdots & \ddots & \vdots \\ R(\boldsymbol{\theta}, \boldsymbol{d}_{m1}) & R(\boldsymbol{\theta}, \boldsymbol{d}_{m2}) & \cdots & R(\boldsymbol{\theta}, \boldsymbol{d}_{mm}) \end{bmatrix} \tag{7}$$

here $\boldsymbol{Y}$ presents the vector of output responses corresponding to the input sample set $\boldsymbol{x} = [\boldsymbol{x}_1, \boldsymbol{x}_2, \cdots, \boldsymbol{x}_m]$; $\boldsymbol{F} = f(\boldsymbol{x}) = [f_1(\boldsymbol{x}), f_2(\boldsymbol{x}), \cdots, f_k(\boldsymbol{x})]$ denotes the vector of $k$ basis functions. By the generalized least squares solution with respect to $\boldsymbol{R}$, the undetermined coefficients $\boldsymbol{\beta}$ is

$$\boldsymbol{\beta} = \left(\boldsymbol{F}^{\mathrm{T}}\boldsymbol{R}^{-1}\boldsymbol{F}\right)^{-1}\boldsymbol{F}^{\mathrm{T}}\boldsymbol{R}^{-1}\boldsymbol{Y} \tag{8}$$

The stochastic component at an untried point $\boldsymbol{x}_*$ is calculated by:

$$Z(\boldsymbol{x}_*) = \boldsymbol{r}^{\mathrm{T}}(\boldsymbol{x}_*)\boldsymbol{R}^{-1}(\boldsymbol{Y} - \boldsymbol{F}\boldsymbol{\beta}) \tag{9}$$

where $\boldsymbol{r}(\boldsymbol{x}_*)$ is the vector of correlations between input samples and untried point $\boldsymbol{x}_*$ and denoted as:

$$\boldsymbol{r}(\boldsymbol{x}_*) = \left[R(\boldsymbol{\theta}, \boldsymbol{d}_{*1}) \quad R(\boldsymbol{\theta}, \boldsymbol{d}_{*2}) \quad \cdots \quad R(\boldsymbol{\theta}, \boldsymbol{d}_{*m})\right] \tag{10}$$

## 2.2 Improved Kriging (IK) algorithm

Improved Kriging (IK) algorithm is developed from Kriging surrogate model and GA method. The GA processes more flexible and adaptive design space exploration, and is hardly affected by the plateau-like function profile of the MLE method, and thus is robust and easily parallelizable for the purpose of computing efficiency [40]. In this study, the GA is applied in the MLE optimization to search the optimal values of the hyperparameter $\boldsymbol{\theta}$ in a Kriging surrogate model, which cannot be optimized by the MLE algorithm with gradient-based counterparts as the shape of its function profile.

The GA approach depends on the natural selection and genetic characteristics, to acquire a new solution of objective function from its initial population by successive multiply iterations with the steps of selection, crossover and mutation [41, 42]. In general, an optimization problem is to search the optimal values to minimize the objective function. When a maximization of an objective function is required, we rewrite this objective function as the negative value of the corresponding function and resolve it in regular way. To compute the hyperparameter $\boldsymbol{\theta}$ in a Kriging surrogate model, the GA method is used to solve the negative value of Eq. (5). This optimization problem is written as

$$\begin{aligned} \min \quad &\varphi(\boldsymbol{\theta}) = \left[\det(\boldsymbol{R})\right]^{\frac{1}{m}} \hat{\sigma}^2 \\ s.t. \quad &\theta^{(j)} > 0, \ j = 1, 2, \cdots, n \end{aligned} \tag{11}$$

The detailed process of obtaining the IK surrogate model is given below. Firstly, the input parameters and objective function are defined and the initial population is generated. The population including the initial population contains many individuals, and each individual is a solution of the objective function. A fitness value obtained by fitness function is utilized to test the quality of the solution and distinguish individuals good or bad in a population. Next, the good individuals are chosen from the previous generation as parents and are applied to generate the next population via the steps of crossover and mutation. Finally, the above two procedures are repeated by successive multiply iterations until the termination criterion is satisfied and the optimal value are obtained. By this way, the optimal values of hyperparameter $\boldsymbol{\theta}$ in a Kriging surrogate model are acquired to establish the IK surrogate model proposed in this paper.

## 2.3　Improved decomposed-coordinated surrogate model method (IDCSMM)

In this sub-section, we elaborate the basic thought of the IDCSMM including ERSM, essential process and the mathematical model of the proposed method.

### 2.3.1　*Extremum response surface method* (*ERSM*)

The dynamic probabilistic analysis of complex structure requires the assessment of dynamic output of analytical objective with regard to the influential factors (i.e., random input variables) in a time domain [0, T]. The structural dynamic probabilistic analysis with the conventional RSM requires establishing a large number of mathematical models of analytical objective in the time domain, so that excess time consumption is needed and even it is difficult to implement the probabilistic evaluation. To efficiently accomplish the structural dynamic probabilistic analysis, ERSM is developed from the response surface method (RSM) and extremum selection method [23, 43], by taking the extreme values from the varying output response of analytical objective. The ERSM is promising to improve the computing efficiency in the dynamic probabilistic analysis of complex structure [22-24]. Generally, the ERSM model with a quadratic polynomial (QP) [44] is expressed as

$$y_{ERSM}(\boldsymbol{x}) = a + \boldsymbol{bx} + \boldsymbol{x}^T \boldsymbol{cx} \tag{12}$$

in which $a$, $\boldsymbol{b}$ and $\boldsymbol{c}$ are the undetermined coefficient of constant term, line term and quadratic term. The forms of $\boldsymbol{b}$, $\boldsymbol{c}$ and $\boldsymbol{x}$ can be expressed as

$$\begin{cases} \boldsymbol{b} = \begin{bmatrix} b_1 & b_2 & \cdots & b_n \end{bmatrix} \\ \boldsymbol{c} = \begin{bmatrix} c_{11} & c_{12} & \cdots & c_{1n} \\ c_{21} & c_{22} & \cdots & c_{2n} \\ \vdots & \vdots & \ddots & \vdots \\ c_{n1} & c_{n2} & \cdots & c_{nn} \end{bmatrix} \\ \boldsymbol{x} = \begin{bmatrix} x_1 & x_2 & \cdots & x_n \end{bmatrix}^T \end{cases} \tag{13}$$

The Eq. (12) can be reshaped as

$$y_{ERSM}(\boldsymbol{x}) = a + \sum_{j=1}^{n} b_j x_j + \sum_{\substack{j=1, l=1 \\ j \neq l}}^{n} c_{jl} x_j x_l + \sum_{j=1}^{n} c_{jj} (x_j)^2 \tag{14}$$

where $l=1, 2, \cdots, n$; $x_j$ and $x_l$ are the values of the $j$-th and $l$-th input variable.

These undetermined coefficients in Eq. (14) are computed with the sample data corresponding to the extreme values of output response：

$$y_{ERSM}(\boldsymbol{x}) = \left\{ y_{p,\max}(\boldsymbol{x}_p), p = 1, 2, \cdots, m \right\} \tag{15}$$

here $y_{p,\max}(\boldsymbol{x}_p)$ represents the extreme value of the $p$-th output response $y_p$ at the moment $t \in [0, T]$.

### 2.3.2 Essential process of IDCSMM

The ERSM is proposed for the probabilistic analysis of single structure and is effective to handle the transient problem. As for the complex structure with many components, however, the ERSM still faces with unacceptable computational precision because the least squares method is only used to establish the ERSM model and cannot precisely handle the high-nonlinearity and large-scale input variables. Besides, the ERSM do not have the ability in handling the probabilistic analysis of multi-component structure since the samples are obtained with multiple repeated sampling from many components. Despite the IK algorithm can provide a significant improvement in nonlinear modeling relative to the QP model, the transients of the structural dynamic reliability and sensitivity assessment cannot be processed effectively. In this case, the IDCSMM is proposed to overcome the above issues in the probabilistic analysis of multi-component structure, by integrating the DC strategy [20, 45], ERSM and IK algorithm. The DC strategy can reduce time consumption and improve computing efficiency in the probabilistic analysis of structures [1, 46]. Along with the heuristic thought, the IDCSMM is employed to the dynamic probabilistic analysis of multi-component structure. The basic procedure is drawn in Fig. 1.

As shown in Fig. 1, it is obvious that the procedure of multi-component structural dynamic probabilistic analysis with IDCSMM mainly incudes dynamic deterministic analysis, parameters optimization, mathematical modeling and dynamic probabilistic analysis. The detailed process of dynamic probabilistic analysis for complex structure with multiple components is summarized as follow.
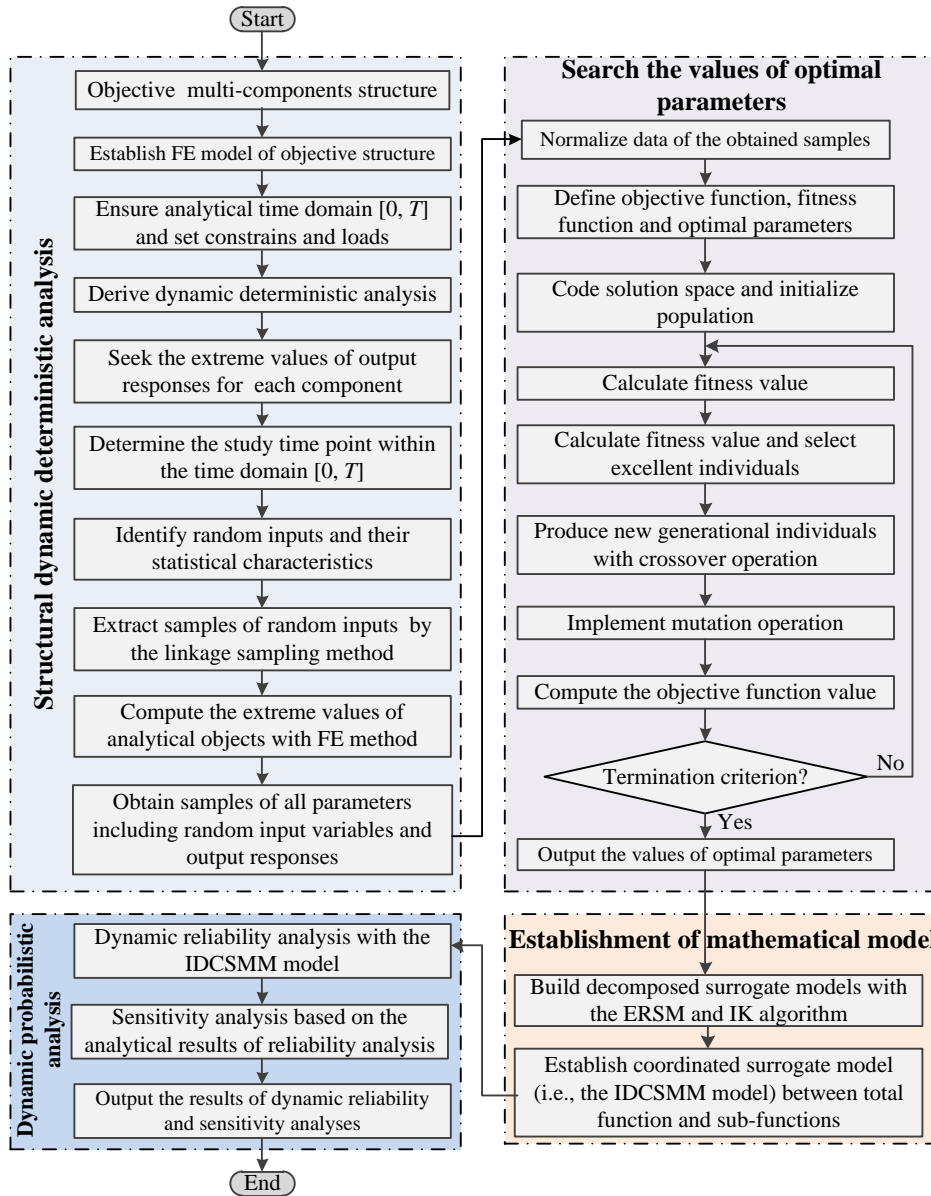
**Fig. 1** The procedure of the dynamic probabilistic analysis of multi-component structures with the IDCSMM

(1) By the FE modeling of this structure and setting boundary constrains and loads, the structural dynamic deterministic analysis is implemented within the time domain $[0, T]$.

(2) Based on the deterministic analyses, the extreme values of output responses of each component are extracted and the study time point is ascertained within the time domain $[0, T]$.

(3) The random inputs and their statistical traits are identified in accordance with engineering practice, and the samples of the random inputs are extracted by using the linkage sampling method. The linkage sampling method developed from the Latin Hypercube Sampling [47], extremum selection method and linkage analysis strategy [48], to obtain the extreme values of multiple analytical objects synchronously via one group sample of random input variables. Considering a random input variable set $x$ and two output responses $y_1$ and $y_2$, the sampling method can be explained by Fig. 2.

(4) The extreme values of analytical objects are calculated with the dynamic deterministic analyses by the FE models, and the samples of all parameters (including random input variables and output responses) are acquired.

(5) Based on the acquired samples of all parameters, the values of optimal parameters (i.e., the hyperparameter $\theta$ in Kriging surrogate model) are searched in the light of GA algorithm, in which termination criterion is set up

depending on generation number.

(6) The decomposed surrogate models of each analytical object are established with the ERSM and IK algorithm, and the coordinated surrogate model (i.e., the IDCSMM model) is built in accordance with the relationship among the analytical object of multi-component structures.

(7) The dynamic reliability and sensitivity analysis is finished with the IDCSMM model.



**Note:**

- The circular (blue marked) and rhombus (red marked) points are the output responses $y_1$ and $y_2$, respectively;

- $x_{low}$ and $x_{up}$ represent the lower and upper values of random input variable set $x$;

- $y_{1,\,low}$, $y_{2,\,low}$ and $y_{1,\,up}$, $y_{2,\,up}$ indicate the lower and upper values of output responses $y_1$ and $y_2$.
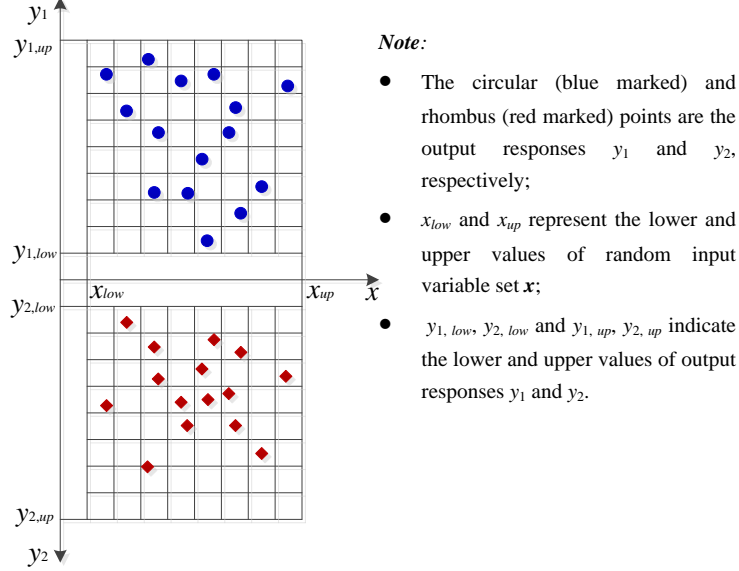
**Fig. 2** The principle of linkage sampling method

### 2.3.3 Mathematical modeling of IDCSMM

The mathematical model of the proposed IDCSMM is discussed for the dynamic probabilistic analysis of multi-component structure in this sub-section. This paper takes four layers (i.e., complex structure layer, first sub-structure layer, second sub-structure layer and variable layer) as an example to study the basic principle of the IDCSMM and establish its model. The decomposed and coordinated schematic diagram of multi-component structure with four layers is drawn in Fig. 3.
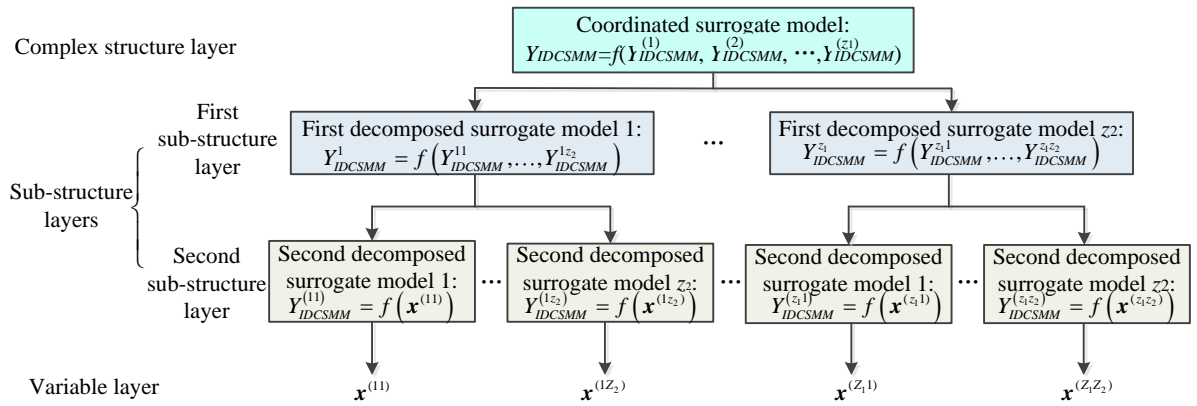


**Fig. 3** The decomposed and coordinated sketch map of four-layer multi-component structure

As demonstrated in Fig. 3, the four-layer complex structure includes $z_1$ ($z_1 \in Z$) first sub-structures and $z_2$ ($z_2 \in Z$) second sub-structures. When $Y_{IDCSMM}(x)$ and $x$ indicate the output response of analytical object and the input variable vector of four-layer complex structure, respectively, the complex structure layer is expressed by

$$Y_{IDCSMM} = f(x) = f\left(f^{(1)}(x), f^{(2)}(x), \cdots, f^{(z_1)}(x)\right) \tag{16}$$

here $f(\cdot)$ represents the complex structure layer function, namely the coordinated surrogate model. Due to $z_1$ first sub-structures, Eq. (16) can be expressed as

$$Y_{IDCSMM} = f\left(Y_{IDCSMM}^{(1)}, Y_{IDCSMM}^{(2)}, \cdots, Y_{IDCSMM}^{(z_1)}\right) \tag{17}$$

in which $Y_{IDCSMM}^{(\tilde{i})}$ $\left(\tilde{i} = 1, 2, \cdots, z_1\right)$ is the $\tilde{i}$-th first decomposed surrogate model. The model of $\tilde{i}$-th first sub-structure layer can be written by

$$Y_{IDCSMM}^{(\tilde{i})} = f\left(Y_{IDCSMM}^{(\tilde{i}1)}, Y_{IDCSMM}^{(\tilde{i}2)}, \cdots, Y_{IDCSMM}^{(\tilde{i}z_2)}\right) \tag{18}$$

here $Y_{IDCSMM}^{(\tilde{i}\tilde{j})}$ $\left(\tilde{j} = 1, 2, \cdots, z_2\right)$ is the $\bar{j}$-th second decomposed surrogate model in the $\tilde{i}$-th first sub-structure layer. This second sub-structure layer contains $z_1 z_2$ second decomposed surrogate models. The function relationship between $Y_{IDCSMM}^{(\tilde{i}\tilde{j})}$ and the variable layer is

$$Y_{IDCSMM}^{(\tilde{i}\tilde{j})} = f\left(x^{(\tilde{i}\tilde{j})}\right) \tag{19}$$

where $x^{(\tilde{i}\tilde{j})}$ indicates the original variable vector of the $\bar{j}$-th second decomposed surrogate model in the $\tilde{i}$-th first sub-structure layer. The relationship between $x$ and $x^{(\tilde{i}\tilde{j})}$ is

$$x = \bigcup_{\tilde{i}=1}^{z_1} \bigcup_{\tilde{j}=1}^{z_2} x^{(\tilde{i}\tilde{j})} \tag{20}$$

According to the DC strategy, the complex structure is divided into multiple sub-structures in different layers. The sub-structure layer functions of different layers (i.e., the first and second decomposed surrogate models) are established with respect to the ERSM and IK algorithm. The complex structure layer function (coordinated surrogate model) is built by the relationship of analytical objects of complex structure and sub-structures.

By Eqs. (1), (12) and (13), the $\tilde{j}$-th second decomposed surrogate model in the $\tilde{i}$-th first sub-structure layer is

$$Y_{IDCSMM}^{(\tilde{i}\tilde{j})}\left(x^{(\tilde{i}\tilde{j})}\right) = y_{ERSM}^{(\tilde{i}\tilde{j})}\left(x^{(\tilde{i}\tilde{j})}\right) + Z\left(x^{(\tilde{i}\tilde{j})}\right) = a^{(\tilde{i}\tilde{j})} + b^{(\tilde{i}\tilde{j})} x^{(\tilde{i}\tilde{j})} + \left(x^{(\tilde{i}\tilde{j})}\right)^T c^{(\tilde{i}\tilde{j})} x^{(\tilde{i}\tilde{j})} + Z\left(x^{(\tilde{i}\tilde{j})}\right)$$

$$s.t. \begin{cases} b^{(\tilde{i}\tilde{j})} = \begin{bmatrix} b_1^{(\tilde{i}\tilde{j})} & b_2^{(\tilde{i}\tilde{j})} & \cdots & b_{\bar{n}}^{(\tilde{i}\tilde{j})} \end{bmatrix} \\ c^{(\tilde{i}\tilde{j})} = \begin{bmatrix} c_{11}^{(\tilde{i}\tilde{j})} & c_{12}^{(\tilde{i}\tilde{j})} & \cdots & c_{1\bar{n}}^{(\tilde{i}\tilde{j})} \\ c_{21}^{(\tilde{i}\tilde{j})} & c_{22}^{(\tilde{i}\tilde{j})} & \cdots & c_{2\bar{n}}^{(\tilde{i}\tilde{j})} \\ \vdots & \vdots & \ddots & \vdots \\ c_{\bar{n}1}^{(\tilde{i}\tilde{j})} & c_{\bar{n}2}^{(\tilde{i}\tilde{j})} & \cdots & c_{\bar{n}\bar{n}}^{(\tilde{i}\tilde{j})} \end{bmatrix} \\ x^{(\tilde{i}\tilde{j})} = \begin{bmatrix} x_1^{(\tilde{i}\tilde{j})} & x_2^{(\tilde{i}\tilde{j})} & \cdots & x_{\bar{n}}^{(\tilde{i}\tilde{j})} \end{bmatrix}^T \end{cases} \tag{21}$$

in which $a^{(\tilde{i}\tilde{j})}$, $b^{(\tilde{i}\tilde{j})}$ and $c^{(\tilde{i}\tilde{j})}$ denote the undetermined coefficient of the constant term, undetermined coefficient vector of the line term and undetermined coefficient matrix of the quadratic term for the $\tilde{j}$-th second decomposed surrogate model in the $\tilde{i}$-th first sub-structure layer, respectively; $\bar{n}$ indicates the number of inputs of the $\tilde{j}$-th second decomposed surrogate model in the $\tilde{i}$-th first sub-structure layer.

In light of Eq. (14), the formula of Eq. (21) may be rewritten as

$$Y_{IDCSMM}^{(\tilde{i}\tilde{j})}\left(\boldsymbol{x}^{(\tilde{i}\tilde{j})}\right)=a^{(\tilde{i}\tilde{j})}+\sum_{\bar{j}=1}^{\bar{n}}b_{\bar{j}}^{(\tilde{i}\tilde{j})}x_{\bar{j}}^{(\tilde{i}\tilde{j})}+\sum_{\substack{\bar{j}=1,\bar{l}=1 \\ \bar{j}\neq\bar{l}}}^{\bar{n}}c_{\bar{j}\bar{l}}^{(\tilde{i}\tilde{j})}x_{\bar{j}}^{(\tilde{i}\tilde{j})}x_{\bar{l}}^{(\tilde{i}\tilde{j})}+\sum_{\bar{j}=1}^{\bar{n}}c_{\bar{j}\bar{j}}^{(\tilde{i}\tilde{j})}\left(x_{\bar{j}}^{(\tilde{i}\tilde{j})}\right)^{2}+Z\left(\boldsymbol{x}^{(\tilde{i}\tilde{j})}\right) \qquad (22)$$

where $\bar{j},\bar{l}=1,2,\cdots,\bar{n}$; $b_{\bar{j}}^{(\tilde{i}\tilde{j})}$ is the undetermined coefficient of the line term of the $\tilde{j}$-th second decomposed surrogate model in the $\tilde{i}$-th first sub-structure layer; $c_{\bar{j}\bar{l}}^{(\tilde{i}\tilde{j})}$ and $c_{\bar{j}\bar{j}}^{(\tilde{i}\tilde{j})}$ are the undetermined coefficients of the quadratic term of the $\tilde{j}$-th second decomposed surrogate model in the $\tilde{i}$-th first sub-structure layer.

The output response $Y_{IDCSMM}^{(\tilde{i}\tilde{j})}\left(\boldsymbol{x}^{(\tilde{i}\tilde{j})}\right)$ of the $\bar{j}$-th second decomposed surrogate model in the $\tilde{i}$-th first sub-structure layer are selected as the input variable $\boldsymbol{x}^{(\tilde{i})}$ in the first sub-structure layer. The relationship function between $\boldsymbol{x}^{(\tilde{i})}$ and $Y_{IDCSMM}^{(\tilde{i}\tilde{j})}\left(\boldsymbol{x}^{(\tilde{i}\tilde{j})}\right)$ is

$$\boldsymbol{x}^{(\tilde{i})}=\left\{Y_{IDCSMM}^{(\tilde{i}\tilde{j})}\left(\boldsymbol{x}^{(\tilde{i}\tilde{j})}\right)\right\} \qquad (23)$$

Referring to establishing the second decomposed surrogate model, the $\tilde{i}$-th first decomposed surrogate model in the first sub-structure layer with quadratic polynomials is expressed as

$$\left\{\begin{aligned}
Y_{IDCSMM}^{(\tilde{i})}\left(\boldsymbol{x}^{(\tilde{i})}\right)&=f\left(\boldsymbol{x}^{(\tilde{i})}\right)=f\left(\left\{Y_{IDCSMM}^{(\tilde{i}\tilde{j})}\left(\boldsymbol{x}^{(\tilde{i}\tilde{j})}\right)\right\}\right)=y_{ERSM}\left(\boldsymbol{x}^{(\tilde{i})}\right)+Z\left(\boldsymbol{x}^{(\tilde{i})}\right)\\
&=a^{(\tilde{i})}+\boldsymbol{b}^{(\tilde{i})}\boldsymbol{x}^{(\tilde{i})}+\left(\boldsymbol{x}^{(\tilde{i})}\right)^{T}\boldsymbol{c}^{(\tilde{i})}\boldsymbol{x}^{(\tilde{i})}+Z\left(\boldsymbol{x}^{(\tilde{i})}\right)\\
\boldsymbol{b}^{(\tilde{i})}&=\left[b_{1}^{(\tilde{i})}\quad b_{2}^{(\tilde{i})}\quad\cdots\quad b_{\hat{n}}^{(\tilde{i})}\right]\\
\boldsymbol{c}^{(\tilde{i})}&=\begin{bmatrix}c_{11}^{(\tilde{i})}&c_{12}^{(\tilde{i})}&\cdots&c_{1\hat{n}}^{(\tilde{i})}\\c_{21}^{(\tilde{i})}&c_{22}^{(\tilde{i})}&\cdots&c_{2\hat{n}}^{(\tilde{i})}\\\vdots&\vdots&\ddots&\vdots\\c_{\hat{n}1}^{(\tilde{i})}&c_{\hat{n}2}^{(\tilde{i})}&\cdots&c_{\hat{n}\hat{n}}^{(\tilde{i})}\end{bmatrix}\\
\boldsymbol{x}^{(\tilde{i})}&=\left[x_{1}^{(\tilde{i})}\quad x_{2}^{(\tilde{i})}\quad\cdots\quad x_{\hat{n}}^{(\tilde{i})}\right]^{T}
\end{aligned}\right. \qquad (24)$$

$$Y_{IDCSMM}^{(\tilde{i})}\left(\mathbf{x}^{(\tilde{i})}\right) = a^{(\tilde{i})} + \sum_{\hat{j}=1}^{\hat{n}} b_{\hat{j}}^{(\tilde{i})} x_{\hat{j}}^{(\tilde{i})} + \sum_{\substack{\hat{j}=1,\hat{l}=1 \\ \hat{j}\neq\hat{l}}}^{\hat{n}} c_{\hat{j}\hat{l}}^{(\tilde{i})} x_{\hat{j}}^{(\tilde{i})} x_{\hat{l}}^{(\tilde{i})} + \sum_{\hat{j}=1}^{\hat{n}} c_{\hat{j}\hat{j}}^{(\tilde{i})} \left(x_{\hat{j}}^{(\tilde{i})}\right)^2 + Z\left(\mathbf{x}^{(\tilde{i})}\right) \tag{25}$$

here $\hat{n}$ represents the number of input variables in the $\tilde{i}$-th first sub-structure layer; $\hat{j}, \hat{l} = 1, 2, \cdots, \hat{n}$; $a^{(\tilde{i})}$, $\mathbf{b}^{(\tilde{i})}$,

$\mathbf{c}^{(\tilde{i})}$, $b_{\hat{j}}^{(\tilde{i}\,\hat{j})}$, $c_{\hat{j}\hat{l}}^{(\tilde{i}\,\hat{j})}$ and $c_{\hat{j}\hat{j}}^{(\tilde{i}\hat{j})}$ are the undetermined coefficients.

Similarly, taking the output response $Y_{IDCSMM}^{(\tilde{i})}\left(\mathbf{x}^{(\tilde{i})}\right)$ as the input parameter $\mathbf{x}$ of the coordinated surrogate

model in the complex structure layer, i.e.,

$$\mathbf{x} = \left\{ Y_{IDCSMM}^{(\tilde{i})}\left(\mathbf{x}^{(\tilde{i})}\right) \right\} \tag{26}$$

The complex structure function (coordinated surrogate models) can be expressed by Eqs. (27) and (28).

$$Y_{IDCSMM}\left(\mathbf{x}\right) = f\left(\mathbf{x}\right) = f\left(\left\{Y_{IDCSMM}^{(\tilde{i})}\left(\mathbf{x}^{(\tilde{i})}\right)\right\}\right) = y_{ERSM}\left(\mathbf{x}\right) + Z\left(\mathbf{x}\right) = a + \mathbf{b}\mathbf{x} + \mathbf{x}^T \mathbf{c}\mathbf{x} + Z\left(\mathbf{x}\right) \tag{27}$$

$$Y_{IDCSMM}\left(\mathbf{x}\right) = a + \sum_{j=1}^{n} b_j x_j + \sum_{\substack{j=1,l=1 \\ j\neq l}}^{n} c_{jl} x_j x_l + \sum_{j=1}^{n} c_{jj}\left(x_j\right)^2 + Z\left(\mathbf{x}\right) \tag{28}$$

Though the above analyses, the DC strategy is to disintegrate complex structure into multiple sub-structures, and the IDCSMM model is built on basis of the ERSM and IK algorithm, which includes the coordinated surrogate model (Eq. (28)) in complex structure layer, the first surrogate model (Eq. (25)) in first sub-structure layer and the second surrogate model (Eq. (22)) in second sub-structure layer. Since the established IDCSMM model is used to replace the true structural model to implement the multi-component structural dynamic probabilistic analysis, it is promising to reduce computing burden and improve computational efficiency. Besides, relative to complex structure, the reduction of the inputs number in the decomposed surrogate models in the sub-structure layer simplifies the complexity of mathematical model, which can effectively reduce nonlinearity and enhance the model approximate accuracy in the probabilistic analysis of multi-component structure.

## 2.4 Dynamic probabilistic analysis

This sub-section discusses the dynamic reliability evaluation and sensitivity analysis for a complex structure with multiple components based on the first and second moment (FOSM) method and Monte Carlo (MC) method [22, 32]. By the coordinated surrogate model in Eq. (28) and the allowable value of the output response for the analytical onjective $Y_{allow}$, the limit state function of multi-component structure is

$$H\left(\mathbf{x}\right) = Y_{allow} - Y_{IDCSMM}\left(\mathbf{x}\right) = Y_{allow} - y_{ERSM}\left(\mathbf{x}\right) - Z\left(\mathbf{x}\right) \tag{29}$$

in which $H(\mathbf{x}) \geq 0$ indicates that the structure is safety, while $H(\mathbf{x}) < 0$ illustrates that the structure is failure.

### 2.4.1 Reliability evaluation method

Based on the FOSM apporach and Taylor's series, the limit state function in Eq. (29) is expanded as

$$H(\boldsymbol{x}) = H(x_1, x_2, \cdots, x_n) = H\left(\mu_{x_1}, \mu_{x_2}, \cdots, \mu_{x_n}\right) + \sum_{j=1}^{n}\left(\frac{\partial H(\boldsymbol{x})}{\partial x_j}\right)_{\boldsymbol{\mu_x}}\left(x_j - \mu_{x_j}\right) \tag{30}$$

where $\boldsymbol{\mu_x} = \left(\mu_{x_1}, \mu_{x_2}, \cdots, \mu_{x_n}\right)$ refers to the mean vector of the $n$ random input variables; $\left(\dfrac{\partial H(\boldsymbol{x})}{\partial x_j}\right)_{\boldsymbol{\mu_x}}$ denotes the

limit state function (Eq. (29)) calculated at the mean value point $\boldsymbol{\mu_x}$. In addition, we assume that the inputs obey a normal distribution and are mutually independent.

In view of the Taylor's series expansion with the limit state function (Eq. (30)), the mean value $\mu_H$ and variance $\sigma_H^2$ of the limit state function in respect to the independent random inputs can be estimated by

$$\mu_H = H(\boldsymbol{\mu_x}) = H\left(\mu_{x_1}, \mu_{x_2}, \cdots, \mu_{x_n}\right)$$

$$\sigma_H^2 = \left(\sum_{j=1}^{n}\left(\frac{\partial H(\boldsymbol{x})}{\partial x_j}\right)_{\boldsymbol{\mu_x}}\left(x_j - \mu_{x_j}\right)\right)^2 = \sum_{j=1}^{n}\left(\frac{\partial H(\boldsymbol{x})}{\partial x_j}\right)_{\boldsymbol{\mu_x}}^2\left(x_j - \mu_{x_j}\right)^2 = \sum_{j=1}^{n}\left(\frac{\partial H(\boldsymbol{x})}{\partial x_j}\right)_{\boldsymbol{\mu_x}}^2 \sigma_{x_j}^2 \tag{31}$$

here $\sigma_{x_j}^2$ is the variance of the $j$-th input variable.

Via the above analyses, the reliability index $\chi$, failure index $P_f$ and reliability $P_r$ of complex structure are

$$\chi = \frac{\mu_H}{\sigma_H} = \frac{H\left(\mu_{x_1}, \mu_{x_2}, \cdots \mu_{x_n}\right)}{\sqrt{\sum_{j=1}^{n}\left(\dfrac{\partial H(\boldsymbol{x})}{\partial x_j}\right)_{\boldsymbol{\mu_x}}^2 \sigma_{x_j}^2}}$$

$$P_f = \Phi(-\chi) \tag{32}$$

$$P_r = 1 - P_f$$

In this function, the symbol $\Phi(\cdot)$ indicates the cumulative density function (CDF) of the standard normal distribution (where the mean value $\mu=0$ and the variance $\sigma^2=1$) and is expressed as

$$\Phi(\chi) = \frac{1}{\sqrt{2\pi}}\int_{-\infty}^{\chi}\exp\left(-\frac{1}{2}s^2\right)ds \tag{33}$$

in which $s = \dfrac{x-\mu}{\sigma}$ is used to transform a normal distribution into a standard normal distribution.

To obtain the numerical features of relevant parameters, according to the Chebyshev theorem and Bemoulli theorem [47] and MC simulation, the failure probability and reliability of complex structure are acquired as

$$P_f = P(H(\boldsymbol{x}) < 0) \approx \frac{N_f}{N}$$

$$P_r = P(H(\boldsymbol{x}) \geq 0) = 1 - P_f \approx 1 - \frac{N_f}{N} \tag{34}$$

where $N$ and $N_f$ are the total number of samples and the total number of failures in Eq. (30) with the given allowable value $Y_{allow}$, respectively.

The MC approach is utilized to approximate the reliability degree of complex structure generally by a large quantity of simulations under considering random inputs, which is a favored methodology for large-scale parameters and high-order problem, because its convergence mainly relies on the number of realizations rather than the scale and order of problem [49, 50]. Besides, the MC method is non-intrusive, hence it is still applicable when the absence of the limit state function of complex structure or this function is too complicated.

### 2.4.2 Sensitivity analysis method

Sensitivity analysis is usually applied to evaluate the relationship between inputs on outputs. The sensitivity of a structure can reflect the influence of the variation of random inputs on the failure probability or reliability degree of the structure. The relevant variables importantly influencing the failure or reliability are found to provide the guidance on structural design [51, 23]. The related measure parameters of sensitivity analysis usually comprise both sensitivity degree $S_d$ and impact probability $I_p$. Sensitivity degree reflects the impact level of a random input parameter on the output response of analytical object. Impact probability reveals how much a random input parameter affects the output response of analytical object with respect to other random input variables. Besides, the sensitivity degrees for random input variables have positive and negative values, which depend on whether the variation of an input has a positive or negative effect on the output response [19, 20].

The sensitivity degree $S_d$ is determined by the partial derivation of failure probability or reliability degree function with regard to the distribution characteristics of random inputs including mean value and standard deviation [52, 53]. The mean value sensitivity $S_{d,j}^{\mu}$ and standard deviation sensitivity $S_{d,j}^{\sigma}$ of the $j$-th input $x_j$ on the failure probability or reliability degree are expressed as

$$S_{d,j}^{\mu} = \frac{\partial P_f}{\partial \mu_{x_j}} = \frac{\partial P_f}{\partial \chi} \frac{\partial \chi}{\partial \mu_{x_j}}$$
$$S_{d,j}^{\sigma} = \frac{\partial P_f}{\partial \sigma_{x_j}} = \frac{\partial P_f}{\partial \chi} \frac{\partial \chi}{\partial \sigma_{x_j}}$$

(35)

Refer to Eq. (32) and the CDF in Eq. (33), the failure probability and reliability functions are

$$P_f = \Phi(-\chi) = 1 - P_r = 1 - \Phi(\chi) = 1 - \frac{1}{\sqrt{2\pi}} \int_{-\infty}^{\chi} \exp\left(-\frac{1}{2}s^2\right) ds$$

(36)

We obtain

$$\frac{\partial P_f}{\partial \chi} = -\frac{1}{\sqrt{2\pi}} \exp\left(-\frac{1}{2}\chi^2\right)$$

(37)

Inputting the reliability index $\chi$ in Eq. (32) into Eq. (37), there is

$$\frac{\partial P_f}{\partial \chi} = -\frac{1}{\sqrt{2\pi}} \exp\left(-\frac{1}{2}\left(\frac{\mu_H}{\sigma_H}\right)^2\right)$$

(38)

The partial derivations of the reliability index $\chi$ to the mean value $\mu_{x_j}$ and the standard deviation $\sigma_{x_j}$ of the $j$-th random input variable are

$$\frac{\partial \chi}{\partial \mu_{x_j}} = \frac{1}{\sigma_H} \left( \frac{\partial H(\boldsymbol{x})}{\partial x_j} \right)_{\boldsymbol{\mu}_x}$$
$$\frac{\partial \chi}{\partial \sigma_{x_j}} = \frac{\sigma_{x_j} \mu_H}{\sigma_H^3} \left( \frac{\partial H(\boldsymbol{x})}{\partial x_j} \right)_{\boldsymbol{\mu}_x}^2 \tag{39}$$

Finally, we might rewrite the mean value sensitivity $S_{d,j}^{\mu}$ and standard deviation sensitivity $S_{d,j}^{\sigma}$ below.

$$S_{d,j}^{\mu} = -\frac{1}{\sqrt{2\pi}\sigma_H} \left( \frac{\partial H(\boldsymbol{x})}{\partial x_j} \right)_{\boldsymbol{\mu}_x} \exp\left( -\frac{1}{2} \left( \frac{\mu_H}{\sigma_H} \right)^2 \right)$$
$$S_{d,j}^{\sigma} = -\frac{\sigma_{x_j} \mu_H}{\sqrt{2\pi}\sigma_H^3} \left( \frac{\partial H(\boldsymbol{x})}{\partial x_j} \right)_{\boldsymbol{\mu}_x}^2 \exp\left( -\frac{1}{2} \left( \frac{\mu_H}{\sigma_H} \right)^2 \right) \tag{40}$$

Similarly, the impact probability $I_p$ is defined as the ratio of the absolute sensitivity degree of one input to the sum of the absolute sensitivity degrees of all inputs [32]. Based on $I_{p,j}^{\mu}$, $I_{p,j}^{\sigma}$ and the mean value and standard deviation, the impact probability of the $j$-th random input parameter is expressed by

$$I_{p,j}^{\mu} = \frac{\left| S_{d,j}^{\mu} \right|}{\sum_{j=1}^{n} \left| S_{d,j}^{\mu} \right|}$$
$$I_{p,j}^{\sigma} = \frac{\left| S_{d,j}^{\sigma} \right|}{\sum_{j=1}^{n} \left| S_{d,j}^{\sigma} \right|} \tag{41}$$

Besides, the impact probability satisfies

$$\sum_{j=1}^{n} I_{p,j}^{\mu} = \sum_{j=1}^{n} I_{p,j}^{\sigma} = 1 \tag{42}$$

In this paper, we select $S_{d,j}^{\mu}$ and $I_{p,j}^{\mu}$ to complete the sensitivity analysis of complex structure with multiple components, because they are considered as the indexes of the mean value sensitivity degree and impact probability of inputs on output of analytical object [22, 23, 49, 52].

From the above analysis, the reliability degree of multi-component structure and the sensitivity of random input parameters on the failure probability are used to assess the design of complex structure with multiply components.

# 3　Case study: dynamic probabilistic analyses of aeroengine turbine blisk

In this section, the dynamic probabilistic analysis of an aeroengine high-pressure turbine blisk with blade and disk is achieved to validate the proposed method (IDCSMM), regarding fluid-thermal-structural interaction.

## 3.1　Finite element modeling

As an important structure of an aeroengine, turbine blisk suffers high pressure, high temperature from combustion chamber, and centrifugal force due to angular speed. The three-dimensional (3-D) model of the blisk with one disk and 48 blades is shown in Fig. 4. Since the turbine blisk is a typical cyclic and symmetric structure, 1/48 turbine blisk model is selected in Fig. 5 as the object of study to reduce computational burden and simulation time. On basis of the geometric model of the turbine blisk, the flow field is generated as displayed in Fig. 6, in which the FTSI surface is the fluid-thermal-structural interaction surface that transfers the fluid and thermal loads to the surface of structure.



(a)　Front view of an aeroengine　　　　(b)　Side view of turbine blisk
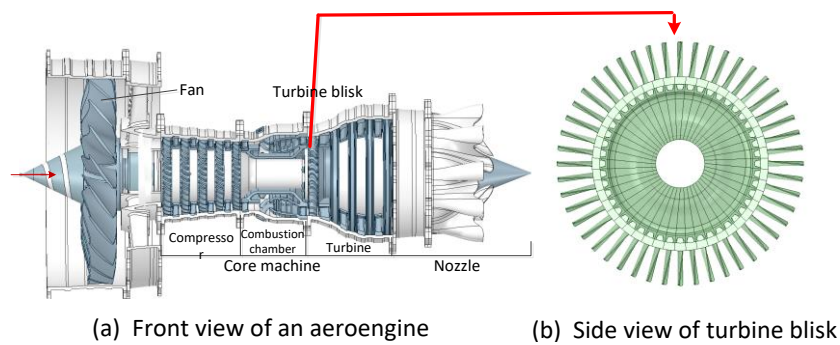
**Fig. 4**　The 3-D model of the high-pressure turbine blisk for an aeroengine
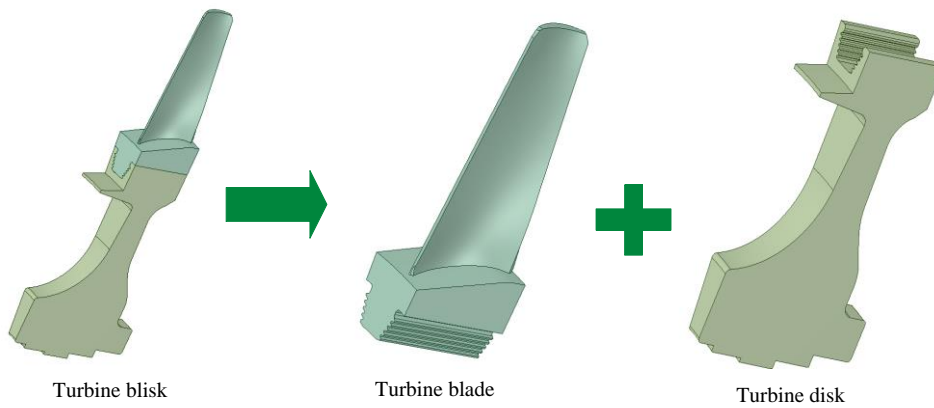


**Fig. 5**　The geometric model of turbine blisk
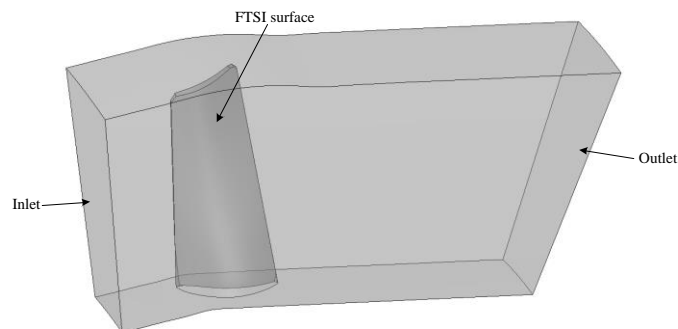


**Fig. 6**　The geometric model of the flow field

In light of the geometric models of the turbine blisk and flow field in Figs. 5-6, the FE model of turbine blisk (with 132 310 nodes and 82 436 tetrahedron elements) and the finite volume(FV) model of flow field (with 472 930 vertices and 338 917 elements) are built as drawn in Fig. 7 and Fig. 8, respectively.



Turbine blade        Turbine disk
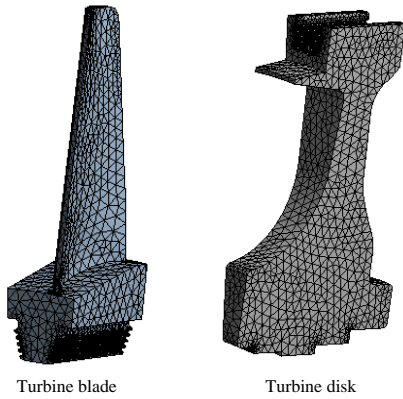
**Fig. 7**    The FE model of turbine blisk
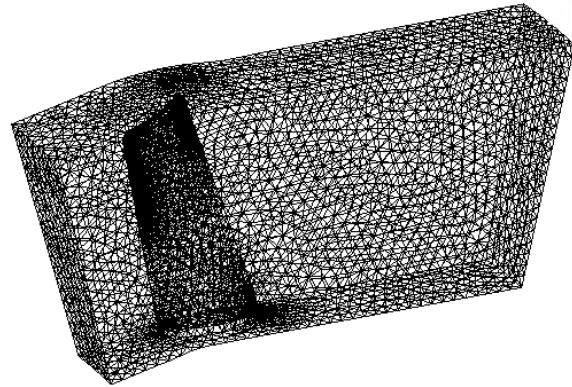


**Fig. 8**    The FV model of the flow field

## 3.2    Input variable selection

As for the blisk, the material is the Nickel-based superalloy GH4133 with the density $8.56 \times 10^3$ kg/m$^3$, Poisson ratio 0.3224 and elastic modulus $1.61 \times 10^{11}$ Pa [21]. The randomness of the input variables is considered including inlet velocity, inlet pressure, outlet pressure, gas temperature, material density and angular speed. The means and standard deviations (Std. Dev.) of random inputs within time domain [0, $T$] are determined via the extremum selection method [43]. We assume that these parameters obey normal distribution and are mutually independent. Their distribution features are listed in Table 1.

**Table 1**    The distribution characteristics of random inputs

| Variables | Mean | Std. Dev. |
|---|---|---|
| Inlet velocity $v$, m/s | 160 | 3.2 |
| Inlet pressure $p_{in}$, Pa | $2 \times 10^6$ | $6 \times 10^4$ |
| Outlet pressure $p_{out}$, Pa | $5.88 \times 10^5$ | $1.76 \times 10^4$ |
| Gas temperature $t$, K | 1 200 | 24 |
| Material density $\rho$, kg/m$^3$ | 8 560 | 171.2 |
| Angular speed $w$, rad/s | 1 168 | 23.36 |

The time domain [0 s, 215 s] is selected for analyzing the blisk radial deformation with the stages of start, idle, take off, climb and cruise [54] as shown in Fig. 9. 12 time points are particularly defined within the time domain and the variations of inlet velocity, gas temperature and angular speed of the blisk with time are drawn in Fig. 9.
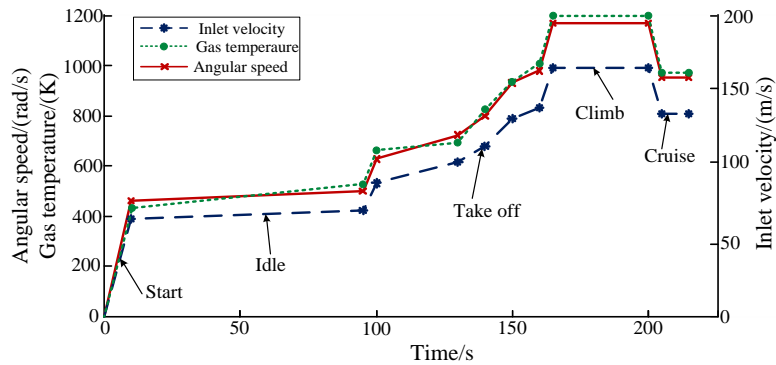


**Fig. 9**    The variations of inlet velocity, gas temperature and angular speed of turbine blisk in [0 s, 215 s]

## 3.3 Dynamic deterministic analysis

For the evaluation of the blisk radial deformation regarding fluid-thermal-structural interaction, we divide fluid-thermal-structural interaction into fluid subsystem, thermal subsystem, structural subsystem and their interdisciplinary coupling. The fluid, thermal and structural analyses are firstly implemented by using the close-coupling analysis method [55]. The relevant analytical parameters contain the material parameters (material density, Poisson ratio, and elastic modulus), boundary conditions (inlet velocity, inlet pressure, outlet pressure, and gas temperature) and angular speed. In view of these inputs in Table 1, the deterministic analysis is completed including fluid analysis setting, thermal analysis setting, structural analysis setting, and iterative solution.

(1) *Fluid analysis setting*    The standard $k$-$\varepsilon$ turbulence model with the FV method is applied to investigate the fluid features of turbine blisk by considering mass and momentum conservation [55, 56].

(2) *Thermal analysis setting*    The laws of energy conservation and heat convection, and solid heat transfer function are employed to perform the thermal analysis of the blisk. The law of energy conservation is to study the thermodynamic property of flow field [21], and the heat convection is to analyze heat transfer on the FTSI surface of fluid and structure, and the solid heat transfer function is to assess the temperature distribution of the blisk [57].

(3) *Structural analysis setting*    The shape equation and displacement function of tetrahedron element and the FE method are employed to implement the structural analysis [58, 59]. The turbine blisk radial deformationis obtained by using the shape equation and displacement function.

(4) *Iterative solution*    Based on the aforementioned steps (1)~(3), the system coupling is considered for the dynamic deterministic analysis for the blisk radial deformation with respect to fluid-thermal-structural interaction by multiple iterations and updating coupling information.

In line with the above analyses, the dynamic deterministic analysis for the turbine blisk with blade and disk is performed based on the close-coupling analysis method. Fig. 10 shows the analytical results of the radial deformation in this time domain [0 s, 215 s].
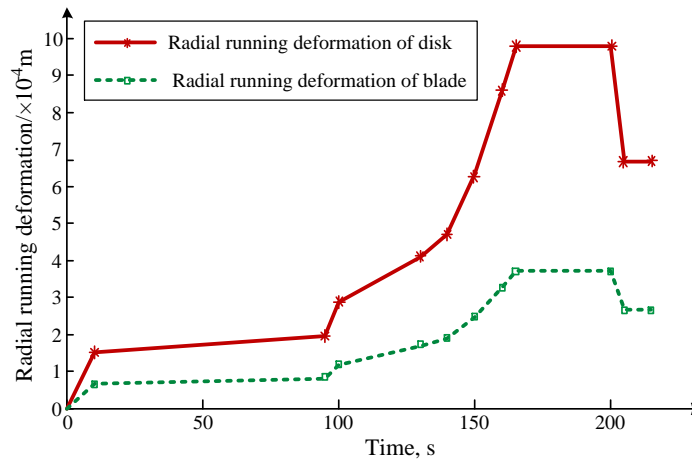


**Fig. 10**    The changing curve of the radial deformations of turbine disk and blade with time

As illustrated in Fig. 10, the radial deformations of blade and disk become larger with the increase of inlet velocity, gas temperature, and angular speed. We also find that the maximum value of the blade and disk radial deformation emerges in the climb phase of the time domain [165 s, 200 s]. The time point $T$=190 s is chosen as the calculation point to investigate the dynamic probabilistic analysis of aeroengine turbine blisk. The pressure distribution of the FTSI surface, the temperature distribution contour plot on turbine blisk and the distribution nephogram of the radial deformation are drawn in Figs. 10~12, respectively, in which $P$ is the pressure of the FTSI surface, and $t_b$ and $t_d$ denote the temperatures of blade and disk, and $u_b$ and $u_d$ indicate the radial deformations of blade and disk. Fig. 13 shows that the maximum radial deformation locates at the top of blade and disk.
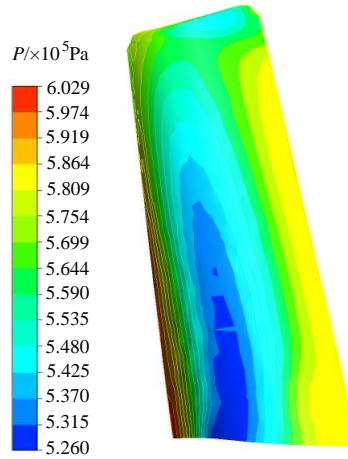
**Fig. 11** The pressure distribution on the FTSI surface



(a) The temperature distribution on blade

(b) The temperature distribution on disk
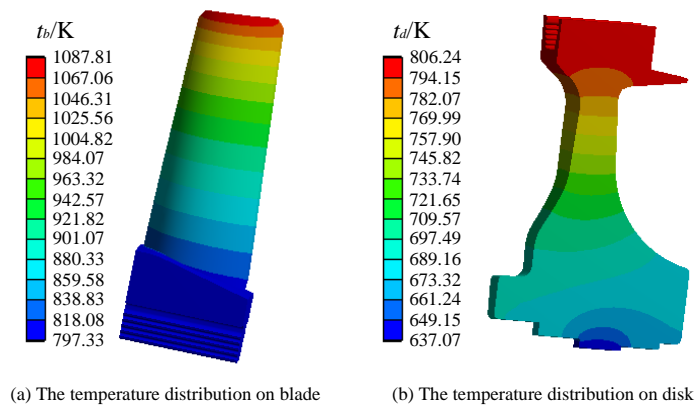
**Fig. 12** The temperature distributions on turbine disk and blade



(a) The distribution nephogram of the radial running deformation of blade

(b) The distribution nephogram of the radial running deformation of disk
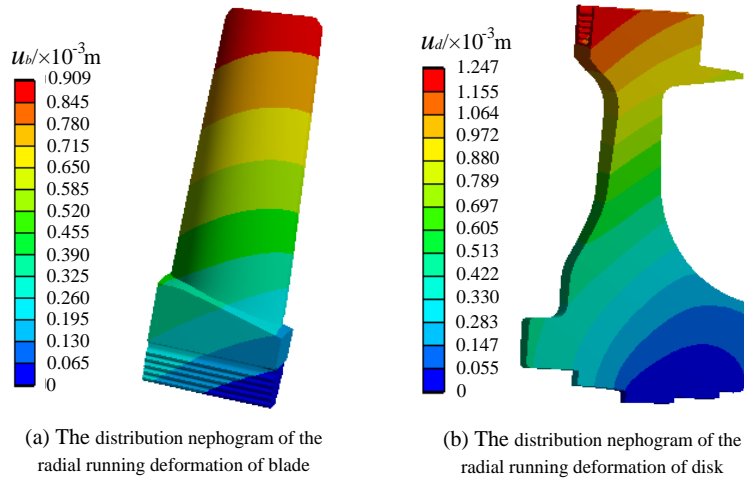
**Fig. 13** The radial deformation distributions of turbine disk and blade

### 3.4 IDCSMM modeling and verification

To establish the IDCSMM model, the 60 samples of the random input variables are extracted based on the dynamic deterministic analyses of turbine blisk with the fluid-thermal-structural interaction. We select 40 samples from the pool of 60 samples as the training samples to establish the IDCSMM model. The remaining 20 samples are regarded as the testing samples to test the accuracy of the modeled IDCSMM model. The detailed process of mathematical modeling is presented in Section 2.3.

To search the hyperparameter $\boldsymbol{\theta}$, the GA follows 120 the size of population, 150 the number of generations, 20 the length of individual, 0.95 the gap of generation, 0.7 crossover probability, and 0.01 mutation probability, by engineering and experience. The evolution processes of blade and disk to find the hyperparameter $\boldsymbol{\theta}$ with two decomposed surrogate models is drawn in Fig. 14.
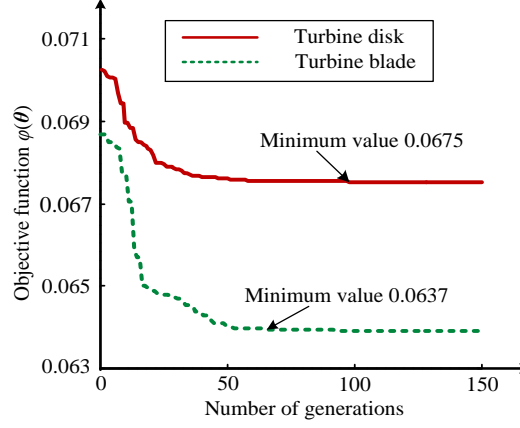


**Fig. 14**  The evolution of objective functions to search the Kriging hyperparameter $\boldsymbol{\theta}$ with the GA

Fig. 14 illustrates that the objective function $\varphi(\boldsymbol{\theta})$ values decrease with the increase of the number of generations in the GA. Moreover, the minimum values for the objective functions of blade and disk reach 0.0637 and 0.0675 at the 62-nd generation. After gaining the optimum hyperparameter $\boldsymbol{\theta}$ in the GA, we can compute the other parameters and undetermined coefficients as shown in Eq.(43) and Eq.(44).

$$
\begin{cases}
a^{(b)} = -0.2747 \\
\boldsymbol{b}^{(b)} = \begin{bmatrix} 0.0136 & 0.0034 & -0.0257 & 0.0300 & 0.9030 & 0.1795 \end{bmatrix} \\
\boldsymbol{c}^{(b)} = \begin{bmatrix}
0.0126 & 0.0368 & -0.0061 & 0.0153 & -0.0336 & 0.0281 \\
0.0368 & 0.1005 & -0.0106 & 0.0098 & -0.0267 & 0.0258 \\
-0.0061 & -0.0106 & 0.0874 & 0.0047 & 0.0109 & 1.8539 \times 10^{-4} \\
0.0153 & 0.0098 & 0.0047 & 0.0769 & -0.0032 & -0.0065 \\
-0.0336 & -0.0267 & 0.0109 & -0.0032 & -0.0118 & -0.0044 \\
0.0281 & 0.0258 & 1.8539 \times 10^{-4} & -0.0065 & -0.0044 & 0.0265
\end{bmatrix} \\
\boldsymbol{\theta}^{(b)} = \begin{bmatrix} 0.1 & 0.1 & 2.4868 & 2.2037 & 3.941 & 18.3705 \end{bmatrix} \\
\boldsymbol{R}^{(b)} = \begin{bmatrix}
1 & 2.0864 \times 10^{-30} & \cdots & 1.1237 \times 10^{-4} \\
2.0864 \times 10^{-30} & 1 & \cdots & 1.0769 \times 10^{-47} \\
\vdots & \vdots & \ddots & \vdots \\
1.1237 \times 10^{-4} & 1.0769 \times 10^{-47} & \cdots & 1
\end{bmatrix} \\
\boldsymbol{r}^{(b)} = \begin{bmatrix} 0.0365 & 0.0066 & -0.3858 & \cdots & -0.3277 & 0.1473 \end{bmatrix}
\end{cases}
\tag{43}
$$

$$
\begin{cases}
a^{(d)} = 0.1830 \\
b^{(d)} = \begin{bmatrix} -0.1536 & -0.0619 & 0.0274 & 0.0704 & 0.7195 & 0.4882 \end{bmatrix} \\
c^{(d)} = \begin{bmatrix}
-0.0479 & -0.0032 & -0.0163 & 0.0604 & 0.0523 & -0.0079 \\
-0.0032 & -0.1223 & 0.0207 & -0.0059 & 0.0262 & -0.0206 \\
-0.0163 & 0.0207 & -0.0573 & -0.0163 & -0.0433 & 0.0292 \\
0.0604 & -0.0059 & -0.0163 & -0.0393 & -0.0098 & -0.0015 \\
0.0523 & 0.0262 & -0.0433 & -0.0098 & 0.0726 & 0.0080 \\
-0.0079 & -0.0206 & 0.0292 & -0.0015 & 0.0080 & -0.0154
\end{bmatrix} \\
\theta^{(d)} = \begin{bmatrix} 0.1 & 0.1 & 2.5008 & 2.2111 & 3.9275 & 18.3837 \end{bmatrix} \\
R^{(d)} = \begin{bmatrix}
1 & 3.1222 \times 10^{-43} & \cdots & 8.9638 \times 10^{-12} \\
3.1222 \times 10^{-43} & 1 & \cdots & 2.4326 \times 10^{-69} \\
\vdots & \vdots & \ddots & \vdots \\
8.9638 \times 10^{-12} & 2.4326 \times 10^{-69} & \cdots & 1
\end{bmatrix} \\
r^{(d)} = \begin{bmatrix} 0.1308 & -0.2855 & 0.5405 & \cdots & -0.3786 & 0.0361 \end{bmatrix}
\end{cases}
\tag{44}
$$

here the superscript symbols $b$ and $d$ denotes turbine blade and disk, respectively.

By the above parameters, we build the IK models $u_{IDCSMM}^{(b)}\left(x^{(b)}\right)$ and $u_{IDCSMM}^{(d)}\left(x^{(d)}\right)$ of blade and disk radial deformations in Eq.(45) and Eq.(46).

$$
u_{IDCSMM}^{(b)}\left(x^{(b)}\right) = a^{(b)} + b^{(b)} x^{(b)} + \left(x^{(b)}\right)^{T} c^{(b)} x^{(b)} + Z\left(x^{(b)}\right)
\tag{45}
$$

$$
u_{IDCSMM}^{(d)}\left(x^{(d)}\right) = a^{(d)} + b^{(d)} x^{(d)} + \left(x^{(d)}\right)^{T} c^{(d)} x^{(d)} + Z\left(x^{(d)}\right)
\tag{46}
$$

in which $x^{(b)} = \left[v^{(b)}, p_{in}^{(b)}, p_{out}^{(b)}, \rho^{(b)}, t^{(b)}, w^{(b)}\right]^{T}$ and $x^{(d)} = \left[v^{(d)}, p_{in}^{(d)}, p_{out}^{(d)}, \rho^{(d)}, t^{(d)}, w^{(d)}\right]^{T}$ are the input variables of turbine blade and disk, respectively.

The total radial deformation of turbine blisk is the sum of turbine blade and disk radial deformations. With Eqs. (43)~(46), the coordinated surrogate model $u_{IDCSMM}^{(bd)}\left(x^{(bd)}\right)$ of the blisk radial deformation is established below.

$$
u_{IDCSMM}^{(bd)}\left(x^{(bd)}\right) = u_{IDCSMM}^{(b)}\left(x^{(b)}\right) + u_{IDCSMM}^{(d)}\left(x^{(d)}\right) = a^{(bd)} + b^{(bd)} x^{(bd)} + \left(x^{(bd)}\right)^{T} c^{(bd)} x^{(bd)} + Z\left(x^{(bd)}\right)
\tag{47}
$$

where $x^{(bd)} = \left[v^{(bd)}, p_{in}^{(bd)}, p_{out}^{(bd)}, \rho^{(bd)}, t^{(bd)}, w^{(bd)}\right]^{T}$ is the inputs of blisk radial deformation.

To validate the proposed method, we use the 60 samples (including 40 training samples and 20 testing samples) to assess the built IDCSMM model. The learning ability and generalization ability of the built IDCSMM model are evaluated by the 40 training samples and 20 testing samples, respectively. As the verification of IDCSMM with 20 testing samples, we compare with the decomposed-coordinated surrogate model (DCSMM)-based quadratic polynomial (QP-DCSMM) and the DCSMM-based Kriging (K-DCSMM based on the standard Kriging model without the GA algorithm). The indexes of evaluations include absolute error $e_{abs}$, relative error $e_{rel}$ and average relative error $e_{ar}$, which are shown in Eq. (48). The testing results from 40 training samples reveal that all errors for

the built IDCSMM model are zero, which explain the good learning ability of the IDCSMM model. The validation results of testing samples are listed in Tables 2.

$$e_{abs}^{(p)} = \left| \left( u_{IDCSMM}^{(bd)} \right)^{(p)} - \left( u^{(bd)} \right)^{(p)} \right|$$

$$e_{rel}^{(p)} = \frac{e_{abs}^{(p)}}{\left( u^{(bd)} \right)^{(p)}} = \frac{\left| \left( u_{IDCSMM}^{(bd)} \right)^{(p)} - \left( u^{(bd)} \right)^{(p)} \right|}{\left( u^{(bd)} \right)^{(p)}} \tag{48}$$

$$e_{ar}^{(i)} = \frac{1}{m} \sum_{p=1}^{m} e_{rel}^{(p)} = \frac{1}{m} \left( \frac{\left| \left( u_{IDCSMM}^{(bd)} \right)^{(p)} - \left( u^{(bd)} \right)^{(p)} \right|}{\left( u^{(bd)} \right)^{(p)}} \right)$$

here $\left( u_{IDCSMM}^{(bd)} \right)^{(p)}$ is the testing response value of the IDCSMM corresponding to the $p$-th sample; $\left( u^{(bd)} \right)^{(p)}$ is the true response value of the FE model corresponding to the $p$-th sample.

As illustrated in Table 2, the errors of the IDCSMM are not equal to zeros in respect of the testing samples. The average relative error of the IDCSMM is 0.675%, which is far less than the average relative errors (2.430% and 1.258%) of the QP-DCSMM and K-DCSMM. The results demonstrates that this proposed method is superior to the conventional method in terms of prediction precision and is a promising tool for the dynamic probabilistic analysis of aeroengine turbine blisk.

### 3.5 Dynamic probabilistic analysis

This sub-section is to implement the dynamic probabilistic analysis (including reliability evaluation and sensitivity analysis) for turbine blisk radial deformation.

#### 3.5.1 Dynamic reliability evaluation

For the dynamic reliability evaluation of the turbine blisk radial deformation, combining with the allowable value according to Eq. (29), the limit state function is shown in Eq. (49). Hereinto, the allowable value is $u_{allow}^{(bd)}$ =2.310×10$^{-3}$ m by engineering experience.

$$h\left( x^{(bd)} \right) = u_{allow}^{(bd)} - u_{IDCSMM}^{(bd)} \left( x^{(bd)} \right) = 2.310 \times 10^{-3} - a^{(bd)} - b^{(bd)} x^{(bd)} - \left( x^{(bd)} \right)^T c^{(bd)} x^{(bd)} - Z\left( x^{(bd)} \right) \tag{49}$$

**Table 2**  The testing results of the IDCSMM with the testing samples

| Sample no. | Output response | | | | Error | | | | | | | | |
|---|---|---|---|---|---|---|---|---|---|---|---|---|---|
| | $u^{(bd)}$, $10^{-3}$ m | $u_{QP}^{(bd)}$, $10^{-3}$ m | $u_{K}^{(bd)}$, $10^{-3}$ m | $u_{IDCSMM}^{(bd)}$ $10^{-3}$ m | $e_{abs,QP}$, $10^{-5}$ m | $e_{rel,QP}$, % | $e_{ar,QP}$, % | $e_{abs,K}$, $10^{-5}$ m | $e_{rel,K}$, % | $e_{ar,K}$, % | $e_{abs}$, $10^{-5}$ m | $e_{rel}$, % | $e_{ar}$, % |
| 1 | 2.325 | 2.114 | 2.076 | 2.323 | 21.16 | 9.103 | | 24.96 | 10.73 | | 2.141 | 0.921 | |
| 2 | 2.206 | 2.208 | 2.235 | 2.212 | 2.292 | 1.039 | | 2.851 | 1.292 | | 0.595 | 0.269 | |
| 3 | 2.177 | 2.175 | 2.178 | 2.169 | 1.325 | 0.608 | 2.430 | 0.150 | 0.069 | 1.258 | 0.687 | 0.316 | 0.675 |
| 4 | 2.161 | 2.148 | 2.138 | 2.135 | 1.257 | 0.582 | | 2.269 | 1.050 | | 2.636 | 1.219 | |
| 5 | 2.165 | 2.146 | 2.117 | 2.134 | 1.871 | 0.865 | | 4.679 | 2.161 | | 3.049 | 1.408 | |
| 6 | 2.219 | 2.228 | 2.229 | 2.244 | 0.912 | 0.411 | | 1.005 | 0.452 | | 2.482 | 1.118 | |

| 7 | 2.105 | 2.111 | 2.115 | 2.118 | 5.501 | 2.613 | 0.986 | 0.468 | 1.221 | 0.580 |
| 8 | 2.284 | 2.274 | 2.276 | 2.282 | 1.003 | 0.439 | 0.716 | 0.313 | 0.230 | 0.101 |
| 9 | 2.116 | 2.141 | 2.134 | 2.131 | 2.506 | 1.184 | 1.823 | 0.861 | 1.571 | 0.742 |
| 10 | 2.096 | 2.160 | 2.136 | 2.139 | 6.417 | 3.062 | 4.024 | 1.919 | 4.293 | 2.048 |
| 11 | 2.236 | 2.244 | 2.244 | 2.241 | 8.038 | 3.594 | 0.795 | 0.355 | 0.478 | 0.214 |
| 12 | 2.291 | 2.281 | 2.299 | 2.285 | 1.061 | 0.463 | 0.808 | 0.352 | 0.595 | 0.259 |
| 13 | 2.167 | 2.181 | 2.174 | 2.177 | 1.395 | 0.644 | 0.727 | 0.335 | 1.054 | 0.486 |
| 14 | 2.203 | 2.215 | 2.219 | 2.214 | 1.203 | 0.546 | 1.567 | 0.711 | 1.051 | 0.477 |
| 15 | 2.162 | 2.132 | 2.136 | 2.139 | 2.999 | 1.387 | 2.532 | 1.172 | 2.297 | 1.062 |
| 16 | 2.198 | 2.203 | 2.190 | 2.189 | 4.819 | 2.192 | 0.808 | 0.368 | 0.924 | 0.420 |
| 17 | 2.201 | 2.189 | 2.183 | 2.191 | 1.141 | 0.518 | 1.797 | 0.816 | 0.981 | 0.446 |
| 18 | 2.249 | 2.226 | 2.224 | 2.225 | 2.341 | 1.041 | 2.478 | 1.102 | 2.463 | 1.095 |
| 19 | 2.241 | 2.231 | 2.239 | 2.234 | 0.974 | 0.435 | 0.265 | 0.118 | 0.688 | 0.307 |
| 20 | 2.183 | 2.190 | 2.194 | 2.183 | 7.552 | 3.459 | 1.118 | 0.512 | 0.038 | 0.017 |

We employ the MC method to run 10 000 simulations on the limit state function of turbine blisk radial deformation to calculate the reliability degree. The simulation history and histogram distributions of turbine blisk radial deformation are drawn in Figs. 15 and 16.
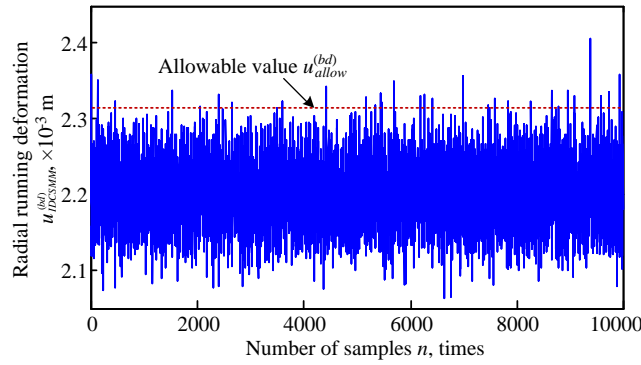


**Fig. 15**   Simulation history of the radial deformation
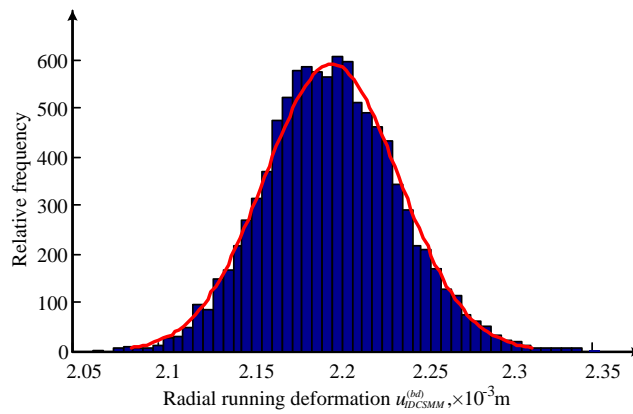


**Fig. 16**   Histogram distribution of the radial deformation

As shown in Figs. 15 and 16, the radial deformation of turbine blisk obeys the normal distribution with the mean $\mu^{(bd)}$=2.200×10⁻³ m and the standard variance $\sigma^{(bd)}$=3.934×10⁻⁵ m. By Eq. (34), the reliability degree of turbine blisk is 0.9949 as the allowable value $u_{allow}^{(bd)}$=2.310×10⁻³ m, which satisfies the requirement of engineering.

### 3.5.2 Sensitivity analysis

Sensitivity analysis is to analyze and quantify the influence of the uncertain degree of input variables on the output response of analytical object, to guide the optimized design of complex structure. In this paper, we utilize the mean value sensitivity in Eq. (40) and impact probability in Eq. (41) to compete the sensitivity indexes considering all random input variables. The results of sensitivity analysis are displayed in Fig. 17 and Table 3.
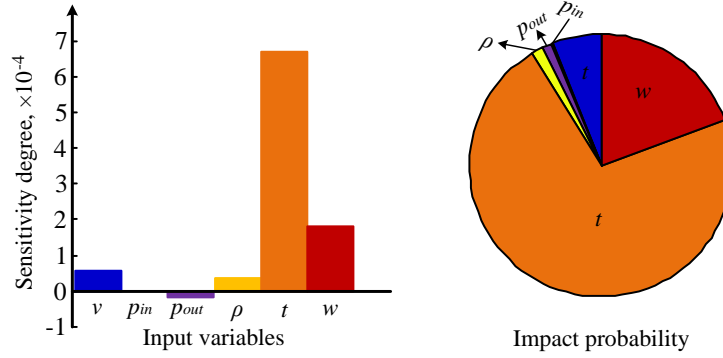


**Fig. 17** The sensitivity results of turbine blisk radial deformation with respect to all input variables

**Table 3** The sensitivity results of all input variables on the turbine blisk radial deformation

| Variable | Inlet velocity $v$ | Inlet pressure $p_{in}$ | Outlet pressure $p_{out}$ | Material density $\rho$ | Gas temperature $t$ | Angular speed $w$ |
|---|---|---|---|---|---|---|
| $s_d^\mu$, $10^{-4}$ | 0.5554 | -0.0232 | -0.1028 | 0.1423 | 6.6598 | 1.8007 |
| $I_p^\mu$, % | 5.98 | 0.24 | 1.11 | 1.53 | 71.73 | 19.41 |

As shown in Fig. 17 and Table 3, the primary affecting the turbine blisk radial deformation is gas temperature, followed by angular speed, inlet velocity, material speed, outlet pressure, and inlet pressure, referring to the pie chart of impact probability. We can also find that the radial deformation of turbine blisk increases with the increase of inlet velocity, material density, gas temperature and angular speed, while with the decrease of inlet pressure and outlet pressure, by the bar graph of input variables and sensitivity degrees. The reason is that the sensitivity degrees of inlet velocity, material density, gas temperature and angular speed are positive values, while the sensitivity degrees of inlet pressure and outlet pressure are negative values. These results are promising to guide the parameter optimization design of turbine blisk.

## 4   The validation of improved decomposed-coordinated surrogate model method

In this section, the effectiveness and applicability of the developed IDCSMM are assessed from model-fitting feature and simulation performance. The model-fitting features are firstly done to verify the IDCSMM performance by comparing with QP-DCSMM and K-DCSMM. By the dynamic reliability analyses of turbine blisk radial deformation, these methods are evaluated referring to the direct simulation (full FE/FV model) with MC method.

### 4.1   Model-fitting features

In this subsection, the effectiveness and feasibility of the IDCSMM is verified which include modelling efficiency and computational accuracy. Therefore, we establish three surrogate models of turbine blisk radial deformation, including the QP-DCSMM model, K-DCSMM model, and IDCSMM model. All calculations are implemented by the same computer in the same computing environment. The 40 groups of inputs are used to build these three surrogate models, which are deemed sufficient for a 6-dimensional fitting problem, and the 20 samples of random input variables are utilized to assess the prediction effects. The model-fitting features of these three surrogate models are summarized in Table 4. Note that the modelling efficiency is determined by the fitting time,

which does not contain the consumption of acquiring samples from the direct simulation, and the computational accuracy is accomplished via the prediction error the average relative error, as listed in Table 3, which can be calculated by using Eq. (48). As for computing the improved precision, we chose the QP-DCSMM as a reference. The reason is that this model is the least precise among these three surrogate models in this paper.

**Table 4**   The model-fitting features for these three surrogate models

| Model | Modelling efficiency, s | Computational accuracy, % | Improved precision, % |
|-------|------------------------|---------------------------|----------------------|
| QP-DCSMM | 2.195 | 2.430 | — |
| K-DCSMM | 0.928 | 1.258 | 1.172 |
| IDCSMM | 0.434 | 0.675 | 1.755 |

The fitting time of the IDCSMM shown in Table 4 is less than those of the QP-DCSMM and K-DCSMM. It is illustrated that the modelling efficiency of the proposed model is superior to those of the QP-DCSMM and K-DCSMM. From the computational accuracy displayed in Table 4, we can see that the prediction error of the IDCSMM is 0.675% and is the lowest among these three surrogate models. Besides, through the information listed in the last column, the QP-DCSMM process the lowest accuracy, while the K-DCSMM and IDCSMM can obviously enhance the prediction precision by 1.172 % and 1.755 % respectively. The developed model has the apparent advantages in terms of modelling efficiency and computational accuracy.

On account of the above observations, it is shown that the developed model is efficient and applicable from the model-fitting features, including the modelling efficiency and computational accuracy. And thus the superiority of the IDCSMM is notable by comparing to the other two surrogate models, which strengthen our confidence to utilize this model to study structural probabilistic analyses and optimization design.

## 4.2   Simulation performance of dynamic reliability analyses

We use the MC simulation to analyze the dynamic reliability degree of aeroengine turbine blisk radial deformation with four different models, which include the direct simulation (i.e., the full FE model with the fluid-thermal-structural interaction) and three surrogate models (i.e., the QP-DCSMM, K-DCSMM, and IDCSMM models) as aforementioned in Sections 3.5 and 4.1. The numerical characteristics of the random input variables are determined by using the values listed in Table 1, and all the calculations and simulation are completed in the same computational environment, by using the MC simulation with these four models. The analytical result of the MC methodology with direct simulation is taken as the reference when we assess the simulation performance, which includes the simulation times and calculative precision for the dynamic reliability analyses of turbine blisk. In this work, we perform different samples, namely $10^2$, $10^3$, and $10^4$ samples, with the MC simulation. However, the MC simulation with $10^4$ samples cannot implement by using the direct simulation. The reason is that the computational burden of this method is too high. The analytical results including the simulation time and calculative precision of the dynamic reliability evaluations of the turbine blisk radial deformation with the four models are listed in Table 6 and table 7, respectively.

**Table 5**   The simulation times of the dynamic reliability analyses of the turbine blisk radial deformation with four models

| Method | Simulation times, s | | |
|--------|---------------------|---|---|
| | $10^2$ samples | $10^3$ samples | $10^4$ samples |
| Direct simulation | 561 600 | 5 724 000 | — |
| QP-DCSMM | 1.79 | 6.38 | 16.52 |
| K-DCSMM | 0.74 | 1.56 | 3.21 |
| IDCSMM | 0.35 | 0.43 | 0.75 |

**Table 6** The calculative precision of the dynamic reliability analyses of the turbine blisk radial deformation with four models

| MC samples | Reliability degree $P_r$ | | | | Calculative precision, % | | |
|---|---|---|---|---|---|---|---|
| | Direct simulation | QP-DCSMM | K-DCSMM | IDCSMM | QP-DCSMM | K-DCSMM | IDCSMM |
| $10^2$ | 0.9900 | 0.9400 | 0.9700 | 0.9900 | 94.95 | 97.98 | 100 |
| $10^3$ | 0.9960 | 0.9890 | 0.9920 | 0.9950 | 99.29 | 99.59 | 99.90 |
| $10^4$ | — | 0.9983 | 0.9935 | 0.9949 | — | — | — |

As revealed in Table 5, the consumption time using these three surrogate models (i.e., the QP-DCSMM, K-DCSMM, and IDCSMM models) is less than using the direct simulation. Among these three surrogate models, the simulation time of the proposed IDCSMM model with the MC method is the most computationally efficient by the comparison with those of the QP-DCSMM and K-DCSMM models.

As shown in Table 6, the dynamic reliability analysis results of the IDCSMM with different samples are the most consistent with the direct simulation based on the full FE model. And the calculative precision of our proposed method is superior to the other two approaches, i.e., the QP-DCSMM and K-DCSMM, for the dynamic reliability assessment for the turbine blisk radial deformation.

Based on the above analytical results, it is demonstrated that the advantages of the developed IDCSMM model as compared to the full FE model and the other two surrogate models, in terms of simulation times and calculative precision, by using the MC method with different samples.

# 5   Conclusions and outlooks

In this work, a novel surrogate modeling method is developed for the dynamic probabilistic analyses for complex structure with multiple components within a time domain [0, $T$]. The proposed method was called as improved decomposed-coordinated surrogate model method (short for, IDCSMM), which fuses the DC strategy, extremum response surface method (ERSM), genetic algorithm (GA) and Kriging model. The GA is integrated into the Kriging model to resolve the maximum likelihood equation (MLE) and obtain the hyperparameter $\theta$. The ERSM is utilized to resolve the transient issue of the response process of complex structure. The DC strategy is used to coordinate the output responses of multi-component structure. To verify the effectiveness and applicability of the developed method, we take an aeroengine turbine blisk, which contains turbine blade and disk, as the case of study by considering the fluid-thermal-structural interaction. According to this effort, some conclusions are drawn as below.

(1) The dynamic deterministic analysis of an aeroengine turbine blisk within the time domain [0 s, 215 s] is investigated to demonstrate the derived model. We acquired the maximums of the turbine blade and disk radial deformations, which are $0.909 \times 10^{-3}$ m and $1.247 \times 10^{-3}$ m.

(2) To derive the surrogate models, we selected six input variables of inlet velocity $v$, inlet pressure $p_{in}$, outlet pressure $p_{out}$, material density $\rho$, gas temperature $t$, and angular speed $w$. As for outputs, we considered the extremum values of the turbine blade and disk radial deformation within the time domain in respect to the principle of ERSM. The surrogate models were established by 40 training samples and verified by 20 testing samples. The 60 samples are obtained by the linkage sampling method. The validation procedure of the derived IDCSMM was finished in modelling efficiency and computational error, by comparing with the DCSMM-based quadratic polynomial (QP-DCSMM) and the DCSMM-based Kriging (K-DCSMM). The analytical results reveal that the modelling efficiency of the developed model is superior to the other two models as the testing error is less than 1%.

(3) When the allowable value is given as $2.310 \times 10^{-3}$ m according to engineering practice, the reliability degree was $P_r$=0.9949, which satisfies the engineering requirements. Besides, we discover that the radial deformation have positive correlations with inlet velocity, material density, gas temperature and angular speed, and negative change

with inlet pressure and outlet pressure. We also find that the highest impact on turbine blisk radial deformation is gas temperature, followed by angular speed, inlet velocity, material density, outlet pressure and inlet pressure. The sensitivity analysis results provide a useful reference for the optimization design of complex structure.

(4) To further verify the developed IDCSMM, we compared the performance of this method to other three methods (i.e., the direct simulation with MC method, QP-DCSMM and K-DCSMM) by the simulation time and calculative precision of the dynamic reliability assessment. The analysis results of the direct simulation were taken as the reference. The simulation times of these methods based the surrogate models are far less than that of the direct simulation. Meanwhile, the consumption time of IDCSMM was superior to other two methods, and the calculative precision of the dynamic reliability evaluation with the proposed method was basically the consistent with that of the direct simulation. The results indicate the high computing efficiency and precision of this method.

In this paper, we provide a novel approach (IDCSMM), to enhance the dynamic reliability evaluation and sensitivity analysis of complex structure in accuracy and efficiency. But some limitations do exist so that we should explore and improve this proposed method in future. In light of the present study and the questions existed, the following suggestions are summarized as follows:

(1) This study uses the dynamic probabilistic analysis of the turbine blisk radial deformation to validate the effectiveness and feasibility of the IDCSMM. However, this method should be verified by applied to more extensive engineering investigations.

(2) Since the optimized results of the GA has no repeatability in solving the Kriging hyperparameter $\boldsymbol{\theta}$, advanced optimization algorithms such as particle swarm optimization, fish swarm algorithm and so forth, or exploring novel optimization algorithms, should be employed to find the relevant parameters to make the model better robustness.

(3) To further improve the application of a novel method, we utilize multiply surrogate models to establish the limit state functions for the multi-component and multi-failure mode analyses of complex structure. The purpose of the investigations is to improve the effects of the dynamic probabilistic analysis of complex structure besides enrich mechanical reliability theory and method.

## Declaration of conflicting interests

The authors declare that there is no conflict of interests regarding the publication of this article.

## Acknowledgments

## References

[1] Bai GC, Fei CW. Distributed collaborative response surface method for mechanical dynamic assembly reliability analysis [J]. Chinese Journal of Mechanical Engineering, 2013, 26(6):1160-1168.

[2] Song LK, Fei CW, Wen J, Bai GC. Multi-objective reliability-based design optimization approach of complex structure with multi-failure modes [J]. Aerospace Science and Technology, 2017, 64:52-62

[3] Whitney DE, Mantripragada R, Adams JD, Rhee S.J. Designing assemblies [J]. Research in Engineering Design-Theory Applications and Concurrent Engineering, 1999, 11(4):229-253.

[4]   Cai JG, Zhou Y, Feng J, Xu Y. Mechanical behavior of a shelter system based on cable-strut structures [J]. Journal of Zhejiang University-Science A, 2012, 13(12):895-903.

[5]   Qian W, Yin X, Xie L, Huang D. Intelligent analysis method of mechanical structure performance [C]. International Forum on Information Technology and Applications, Chengdu, China, MAY 15-17, 2009.

[6]   Salehyar S, Li Y, Zhu Q. Fully-coupled time-domain simulations of the response of a floating wind turbine to non-periodic disturbances [J]. Renewable Energy, 2017, 111:214-226.

[7]   Demoly F, Matsokis A, Kiritsis D. A mereotopological product relationship description approach for assembly oriented design [J]. Robotics and Computer-Integrated Manufacturing, 2012, 28(6):681-693.

[8]   Liu T, Cao Y, Wang J, Yang J. Assembly error calculation with consideration of part deformation [C]. 14th CIRP Conference on Computer Aided Tolerancing, Gothenburg, Sweden, MAY 18-20, 2016.

[9]   Khorrami H, Rakheja S, Sedaghati R. Vibration behavior of a two-crack shaft in a rotor disc-bearing system [J]. Mechanism and Machine Theory, 2017, 113:67-84.

[10]  Huang Y, Yang S, Zhang F, Zhao C, Ling Q, Wang H. Non-linear torsional vibration characteristics of an internal combustion engine crankshaft assembly [J]. Chinese Journal of Mechanical Engineering, 2012, 25(4):797-808.

[11]  Chakravarthy A, Evans KA, Kuhn LM, et al. Frequency and time domain analysis of an aeroelastic wing multiple component structure [J]. Numerical Functional Analysis and Optimization, 2015, 36(9):1122-1152.

[12]  Ma H, Yin F, Wu Z, Tai X, Wen B. Nonlinear vibration response analysis of a rotor-blade system with blade-tip rubbing[J]. Nonlinear Dynamics, 2016, 84(3):1225-1258.

[13]  Birnbaum ZW, Esary JD, Saunders SC. Multi-component systems and structures and their reliability [J]. Technometrics, 1961, 3(1):55-71.

[14]  Gheisi A, Naser G. A surrogate measure for multi-component failure based reliability analysis of water distribution systems [C]. 16th International Conference on Water Distribution System Analysis, Bari, Italy, Jul 14-17, 2014.

[15]  Gao XL, Cui LR, Li JL. Analysis for joint importance of components in a coherent system [J]. European Journal of Operational Research, 2007, 182(1):282-299.

[16]  Schottl A. A reliability model of a system with dependent components [J]. IEEE Transactions on Reliability, 1995,45(2):267-271.

[17]  Song S, Coit D, Feng QM, Feng H. Reliability analysis for multi-component systems subject to multiple dependent competing failure processes [J]. IEEE Transactions on Reliability, 2014, 63(1):331-345.

[18]  Heydt GT, Graf TJ. Distribution system reliability evaluation using enhanced samples in a Monte Carlo approach [J]. IEEE Transactions on Power Systems, 2010, 25(4):2006-2008.

[19]  Fei CW, Choy YS, Hu DY, Bai GC, Tang WZ. Dynamic probabilistic design approach of high-pressure turbine blade-tip radial running clearance [J]. Nonlinear Dynamics, 2016, 86(1):205-223.

[20]  Fei CW, Bai GC, Distributed collaborative probabilistic design for turbine blade-tip radial running clearance using support vector machine of regression [J]. Mechanical Systems and Signal Processing, 2014, 49(1-2): 196-208.

[21]  Gao H, Fei C, Bai G, Ding L. Reliability-based low-cycle fatigue damage analysis for turbine blade with thermo-structural interaction [J]. Aerospace Science and Technology, 2016, 49:289-300.

[22]  Zhang CY, Bai GC. Extremum response surface method of reliability analysis on two-link flexible robot manipulator [J]. Journal of Central South University, 2012, 19(1):101-109.

[23]  Fei CW, Bai GC, Tian C. Extremum response surface method for casing radial deformation probabilistic analysis [J]. Journal of Aerospace Information System, 2013, 10(1):47-52.

[24]  Fei CW, Bai GC. Nonlinear dynamic probabilistic analysis for turbine casing radial deformation based on extremum response surface method-based support vector machine [J]. Journal of Computational and Nonlinear Dynamics, 2013, 8(4): 041004-1-041004-8.

[25]  Fei CW, Tang WZ, Bai GC. Novel method and model for dynamic reliability optimal design of turbine blade deformation [J]. Aerospace Science and Technology, 2014, 39:588-595.

[26] Fei CW, Choy YS, Hu DY, Bai GC, Tang WZ. Transient probabilistic analysis for turbine blade-tip radial clearance with multi-component and multi-physics fields based on DCERSM [J]. Aerospace Science and Technology, 2017, 50:62-70.

[27] Krige DG. A statistical approach to some basic mine valuation problems on the Witwatersran [J]. Journal of the Chemical, Metallurgical and Mining Society of South Africa, 1951, 52:119-139.

[28] Matheron G. The intrinsic random function and their application [J]. Advances in Applied Probability, 1973, 5(3):439-468.

[29] Zhang L, Zhang JY, Li T, Zhang Y. Multi-objective aerodynamic optimization design of high-speed train head shape[J]. Journal of Zhejiang University-Science A, 2017, 18(11):841-854.

[30] Hu DY, Yang JJ, Fei CW, Wang RQ, Choy YS. Reliability-based design optimization method of turbine disk with transformed deterministic constraints [J]. Journal of Aerospace Engineering, 2016, 30(1): 04016070.

[31] Liu HT, Cai JF, Ong YS. An adaptive sampling approach for Kriging metamodeling by maximizing expected prediction error [J]. Computers & Chemical Engineering, 2017, 106:171-182.

[32] Lu C, Feng YW, Rhea. P Liem, Fei CW. Improved kriging with extremum response surface method for structural dynamic reliability and sensitivity analyses [J]. Aerospace Science and Technology, 2018, 76:164-175.

[33] Gao HY, Hu XF, Han F, Li X, Zhang J. Experimental study of Kriging-based crack identification in plate structure [J]. Proceedings of the Institution of Mechanical Engineers Part C-Journal of Mechanical Engineering Science, 2017, 231(17):3118-3129.

[34] Dubourg V, Sudret B, Bourinet JM. Reliability-based design optimization using Kriging surrogate and subset simulation [J]. Structural and Multidisciplinary Optimization, 2011, 44(5):673-690.

[35] Shi Y, Lu ZZ, Li Z, Wu M. Cross-covariance based global dynamic sensitivity analysis [J]. Mechanical Systems and Signal Processing, 2018, 100:846-862.

[36] Liem RP, Mader CA, Martins JRRA. Surrogate models and mixtures of experts in aerodynamic performance prediction for aircraft mission analysis [J]. Aerospace Science and Technology, 2015, 43:126-151.

[37] Sun ZL, Wang J, Li R, Tong C.: A new Kriging based learning function and its application to structural reliability analysis [J]. Reliability Engineering and System Safety, 2017, 157:152-165.

[38] Echard B, Gayton N, Lemaire M, Relun N. A combined importance sampling and Kriging reliability method for small failure probabilistic with time-demanding numerical models [J]. Reliability Engineering and System Safety, 2013, 111:232-240.

[39] Kajeri OT, Thorpe RB, Chen T, Wang B. Kriging meta-model assisted calibration of computational fluid dynamics models [J]. Aiche Journal, 2016, 62(12):4308-4320.

[40] Coello CAC, Pullido GT. Multiobjective structural optimization using a microgenetic algorithm [J]. Structural and Multidisciplinary, 2005, 30(5):388-403.

[41] Agapie A, Wright AH. Theoretical analysis of steady state genetic algorithms [J]. Applications of Mathematics, 2014, 59(5):509-525.

[42] Song LK, Wen J, Fei CW, Bai GC, Distributed collaborative probabilistic design of multi-failure structure with fliud-structure internaction using fuzzy neural network of regression [J]. Mechanical Systems and Signal Processing, 2018, 104: 72-84.

[43] Fei CW, Bai GC. Extremum selection method of random variables for nonlinear dynamic reliability analysis turbine blade deformation [J]. Propulsion and Power Research, 2012, 1(1):58-63.

[44] Fei CW, Bai GC. Distributed collaborative extremum response surface method for mechanical dynamic assembly reliability analysis [J]. Journal of Central South University, 2013, 20 (9): 2414-2422.

[45] Adomian G. A review of the decomposition method in applied mathematics [J]. Journal of Mathematical Analysis and Applications, 1988, 135:501-544.

[46] Fei CW, Bai GC, Tang WZ. Probabilistic design of HPT blade-tip radial running clearance with distributed collaborative response surface method [J]. Journal of Aerospace Engineering, 2015, 28(2):04014069.

[47] Olsson A, Sandberg G, Dahlblom O. On Latin hypercube sampling for structural reliability analysis [J]. Structural Safety, 2003, 25(1):47-68.

[48] Gupta SK, Schaffer AA; Cox AL, Dwarkadas S, Zwaenepoel W. Integrating parallelization strategies for linkage analysis [J]. Computers and Biomedical Research, 1995, 28(2):116-139.

[49] Nielsen A. The Monte Carlo computation error of transition probabilities [J]. Statistics & Probability Letters, 2016, 118:163-170.

[50] Fishman GS. Monte Carlo: concepts, algorithms, and applications [M]. New York: Springer‑Verlag, 1996.

[51] Zhang CY, Song LK, Fei CW, Hao GP, Liu LJ. Reliability-based design optimization for flexible mechanism with particle swarm optimization and advanced extremum response surface method [J]. Journal of Central South University, 2016, 23(8):2001-2007.

[52] Lu ZZ, Song FF, Yue ZF, Wang J. Reliability sensitivity method by line sampling [J]. Structural Safety, 2008, 30(6):517–532.

[53] Zhou CC, Lu ZZ, Hu JX, Yuan M. Response CDF sensitivity and its solution based on sparse grid integration [J]. International Journal of Systems Science, 2016, 47(3):603-616.

[54] Lattime SB, Steinetz BM. Turbine engine clearance control systems: current practices and future directions [J]. Journal of Propulsion and Power, 2004, 20(2):302-311.

[55] Lu C, Feng YW, Fei CW, Xue AF. Probabilistic analysis method of turbine blisk with multi-failure modes by two-way fluid-thermal-solid coupling [J]. Proceedings of the Institution of Mechanical Engineers Part C-Journal of Mechanical Engineering Science, 2017, DOI: 10.1177/0954406217723673.

[56] Patel Y, Patel G, Turunen ST. Influence of turbulence modelling on non-equilibrium condensing flows in nozzle and turbine cascade [J]. International Journal of Heat and Mass Transfer, 2015, 88:165-180.

[57] Ait-Table T, Abdelbaki A, Zrikerm Z. Simulation of coupled heat transfers in a hollow tile with two vertical and three horizontal uniform rectangular cavities heated from below or above [J]. Energy Build, 2014, 84:628-632.

[58] Liu J, Nan Z, Yi P. Validation and application of three-dimensional discontinuous deformation analysis with tetrahedron finite element meshed block [J]. Acta Mechanica Sinica, 2012, 28(6):1602-1616.

[59] Feng H, Cui XY, Li GY, Feng SZ. A temporal stable node-based smoothed finite element method for three-dimensional elasticity problems [J]. Computational Mechanics, 2014, 53(5):859-876.